Chapter 3

PHOTOELECTROLYSIS

3.1 General Description of Photoelectrolysis

Electrolysis is a process of detaching or dissociating bonded elements and compounds by passing through them an electric current. Water electrolysis decomposes H_2O into hydrogen and oxygen gas. Care must be taken in choosing the correct electrolytes, nominally substances that contain free ions and hence behave as an electrically conductive medium. Electrolytes dissolve and dissociate into cations (positive ions, +) and anions (negative ions, −) that carry the current. As we have seen in Chapter 2, such processes can occur in an electrolysis cell, or electrolyzer, which consists of two electrodes, cathode and anode, where reduction and oxidation reactions simultaneously take place forming H_2 (at the cathode) and O_2 (at the anode). The fundamental problem in hydrogen production by water electrolysis is that today the electricity used to drive the process is primarily generated by the burning of fossil fuels.

Photoelectrolysis describes electrolysis by the direct use of light; that is to say, the conversion of light into electrical current and then the transformation of a chemical entity (H_2O, H_2S, etc.) into useful chemical energy (such as H_2) using that current. A photoelectro-chemical cell is used to carry out the various photoelectrolytic reactions, being comprised of a semiconductor device that absorbs solar energy and generates the necessary voltage to split water molecules. Photoelectrolysis integrates solar energy collection and water electrolysis into a single photoelectrode, and is considered the most efficient renewable method of hydrogen production. Our interest in hydrogen stems from it being an energy source that, like fossil fuels, are energy dense and can be readily transported and stored, but unlike fossil fuels is not of finite supply and its combustion does not result in pollution nor the release of climate altering gases.

3.1.1 Photoelectrolysis and the Hydrogen Economy

It appears the term "Hydrogen Economy" became part of the common vernacular in 1974 during the first international conference on hydrogen energy in Miami, Florida signifying the concept of a renewable, non-polluting energy infrastructure based on hydrogen [1]. The underlying premise of a hydrogen economy is the ability to renewably, cleanly, and efficiently produce hydrogen. Photoelectrolysis is a single step process in which sunlight is absorbed by a semiconductor, with the resulting photo-generated electron-hole pair splitting water into hydrogen and oxygen. At present non-renewable hydrogen production methods, such as steam reforming of methane (SMR), are less expensive than photoelectrolysis. Of course SMR results in CO_2 emissions, and is ultimately limited by the finite reserves of fossil fuels. In contrast, water photoelectrolysis does not result in CO_2 emissions, sunlight and water can be considered inexhaustible resources, and as solar-to-hydrogen efficiencies increase it can be expected that the intrinsic costs will continue to decrease. For example the relatively recent advances in nanotechnology have given the scientific community an opportunity to design and synthesize specific semiconductor nanostructures with previously unseen properties. As illustrated by **Fig. 3.1**, photoelectrolysis offers the world a permanent energy solution, one that is both sustainable and pollution free.

3.1.2 Background and Perspectives: Artificial Photosynthesis

The atmosphere of earth is largely composed of nitrogen gas (78%), with other major gases including oxygen (21%), argon (0.93%), and carbon dioxide (0.04%). Plants and some bacteria release oxygen through a process called *Photosynthesis* [2,3]. Photosynthesis, see reaction 3.1.1, is an efficient method of transforming solar energy into chemical energy in the form of starch or sugar.

$$6CO_2 + 12H_2O + \text{solar light} \rightarrow C_6H_{12}O_6 + 6O_2 + 6H_2O \qquad (3.1.1)$$

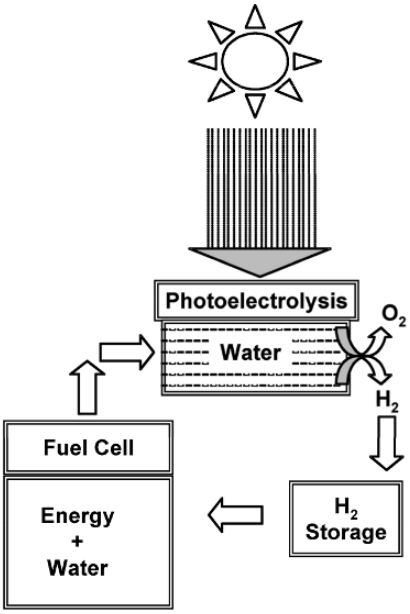

Fig. 3.1: Solar hydrogen production via photoelectrolysis, with enormous potential for providing a renewable and clean energy carrier.

Photosynthesis is the way a plant makes fuel, that is to say useful energy, for itself. There are two types of photosynthetic reaction centers, Photosystem I and Photosystem II, that signify the arrangement of *chlorophyll a* and other pigments packed in a thylakoid membrane. Photosystem I absorbs light at 700 nm and is commonly referred to as P_{700}, while Photosystem II absorbs light at 680 nm and is commonly referred to as P_{680}. Upon activation by solar light an electron is removed from P_{680}, making it sufficiently electronegative to withdraw electrons from water. This electron travels via a cascade of electron carriers to Photosystem I, where $NADP^+$ (oxidized nicotinamide adenine dinucleotide) is reduced to NADPH (reduced nicotinamide adenine dinucleotide). This process generates a redox potential, or energy rich state, across the thylakoid membrane. This potential helps drive the hydrogen ion through the protein channels leading to generation of ATP (adenosine triphosphate) from ADP (adenosine diphosphate). The outcome of this electron transport is that water is split into oxygen gas and hydrogen ions. Although the primary photoredox reactions in the chloroplast

proceed with high quantum efficiency it saturates at modest light intensity, leading to an overall peak illumination photochemical conversion yield of about ≈ 6%. Taking into account seasonal variations, i.e. winter, and its affect on photosynthesis efficiency the result is that biological systems, in comparison to solar cells, are a rather low efficiency method of converting solar energy [4-6].

The idea of constructing an artificial device capable of converting solar energy by mimicking the natural photosynthesis conversion of sunlight into a useful energy is a major driving force in artificial photosynthesis research. Ideally, we seek efficient light induced reactions to split water into molecular oxygen and hydrogen, a process often referred to as artificial photosynthesis [7]. One wishes to be able to mimic the electrochemical energy conversion achievable in photosynthesis, illustrated in **Fig. 3.2a** [7-10]. When light falls on Chlorophyll P_{680} an electron moves from water to the acceptor plastquinone (Q) via pheophytin (Q_A) and secondary quinonone (Q_B) making, in combination with CO_2, sugar (carbohydrate). Electron transport is aided by the presence of four Manganese (Mn) metal atoms in Photosystem II. The photo-ejected electron from P_{680} is replenished by taking one from the Mn cluster through the redox active tyrosine linkage (or mediator), which in turn extracts an electron from water. P_{680} generates an oxidizing potential of + 1.2 V, sufficient to overcome the energy barrier required to oxidize water to molecular oxygen (0.87 V, pH = 6).

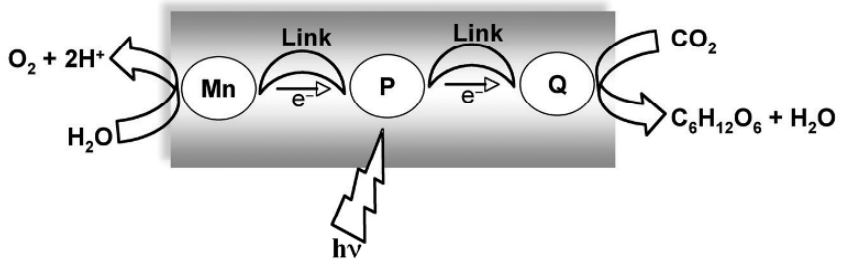

Fig. 3.2a: Electron transport in (natural) photosynthesis. P = chlorophyll that acts as a light sensitizer, from which a photogenerated electron travels to Q = Plastquinone that in combination with CO_2 forms a carbohydrate. The photo-ejected electron from P_{680} is replenished by taking one from the Mn cluster through the redox active tyrosine linkage (or mediator), which in turn extracts an electron from water.

Photosynthesis is a form of photoelectrolysis [11], with the molecular arrangement in the thylakoid membranes creating a photovoltage, resulting in water oxidation on one end of the membrane and reduction on the other. Attempts to successfully achieve artificial photosynthesis via a robust, durable and photoactive supermolecule capable of efficient electron transport, and thus water splitting, have yet to be realized, see **Fig. 3.2b**. The efficiency of artificial systems are currently limited by the poor light absorption achievable in a thin layer of photoactive molecules, while a thin layer is needed to prevent energy losses in electron transport through a membrane. This is in contrast to the thylakoid membranes, in which the P_{680} and P_{700} systems are embedded, that fold upon each other in a disk-like stack resulting in a structure that efficiently harvests sunlight while preventing back reactions.

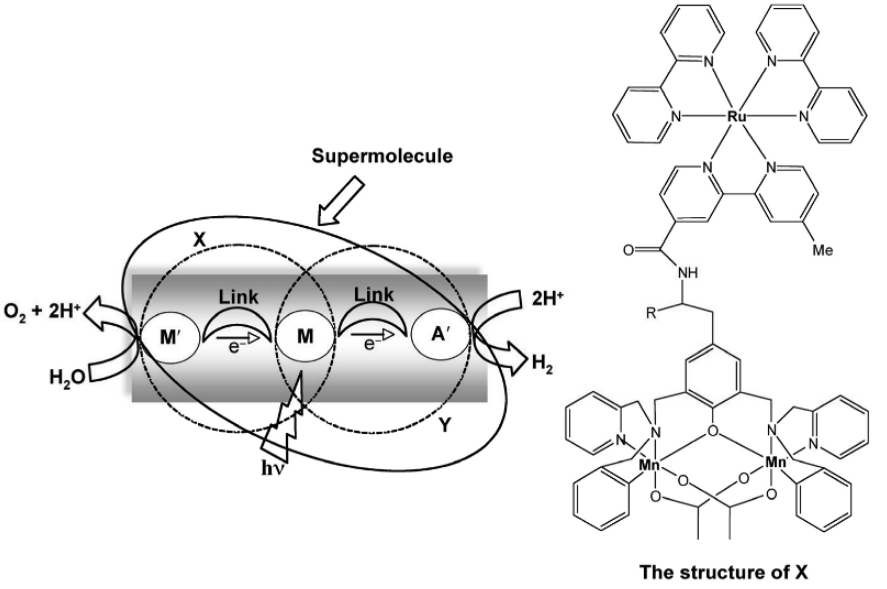

Fig. 3.2b: Electron transport in an artificial photosynthesis scheme. M = light sensitizer, M' = a water oxidation site, and A' = a reduction site.

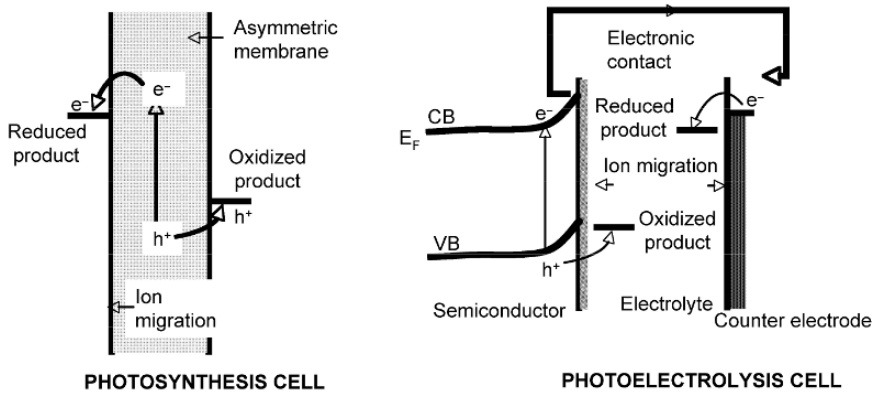

Fig. 3.3: A comparison between photosynthesis and photoelectrolysis in terms of electron transfer reactions.

Figure 3.3 illustrates the relationship between photosynthesis and photoelectrolysis in terms of the redox energy for water splitting. In a photosynthesis cell, both electronic and ionic currents pass through the membrane in parallel. Semiconductor electrodes form the basis of water splitting by photoelectrolysis, with a counter electrode collecting one of the charge carriers generated by an illuminated semiconductor.

3.2 Photoelectrochemical Cells

A cell that can convert light energy into a more useful energy product through light-induced electrochemical processes is commonly known as a *Photoelectrochemical Cell* (PEC). In a photoelectrochemical cell current and voltage are simultaneously produced upon absorption of solar light by one or more of the electrodes, with at least one of the electrodes a semiconductor. The output product is either electrical or chemical energy. Some PECs have been used to produce harmless chemicals from hazardous wastes [12-16].

A typical PEC, as depicted in **Fig. 3.4a** for water splitting, consists of three electrodes immersed in an electrolyte solution; namely the working electrode (WE) or anode, counter electrode (CE) or cathode, and reference electrode (RE). The working electrode, usually a semiconductor, is also called the photoelectrode

or photoanode due to the light induced chemical reactions initiated at its surface. The counter electrode or cathode used for this cell is typically a corrosion resistant metal, commonly platinum, to prevent dissolution products from the counter electrode contaminating the solution.

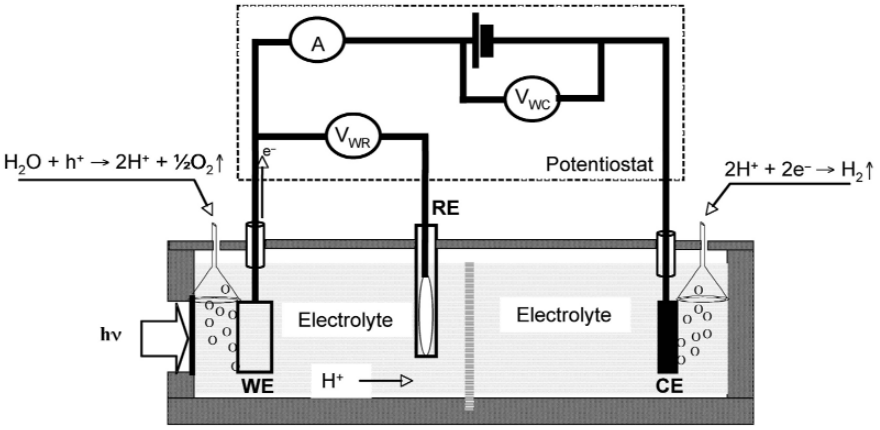

Fig. 3.4a: Schematic representation of a conventional three-electrode photoelectrochemical cell showing: WE = working electrode, RE = reference electrode, CE = counter electrode. If the working electrode is an n-type semiconductor and the counter electrode is a metal, then oxygen evolution occurs at the WE and hydrogen evolution occurs at the CE.

In a common photoelectrochemical cell design, an n-type semiconductor photoanode is used that upon illumination evolves oxygen, while hydrogen is evolved at a metal cathode. Photoelectrochemical cells of other configurations can also be prepared. A p-type semiconductor cathode, or photocathode, reduces the H^+ ion into H_2 upon solar light irradiation, while oxygen is evolved at a metal anode. In another photoelectrochemical cell design both electrodes are comprised of photoactive semiconductors. In this case, the n-type electrode will act as a photo-anode for water oxidation and release of the H^+ ion; the p-type electrode will act as the photo-cathode, where H^+ ions are reduced to H_2. A standard calomel electrode filled with a saturated KCl solution is commonly used as a reference electrode for these cells when an external bias is needed. During use KCl solution from the electrode flows extremely

slowly into the cell through a fine channel in the base of the electrode, providing electrical contact to the cell for characterization without reference electrode contamination. The level of the KCl solution in the electrode needs to remain higher than that of the electrolyte solution in the cell.

3.2.1 Water Splitting

As shown in **Fig. 3.4b**, when a semiconductor electrode is illuminated with photons having an energy hν equal to or larger than the semiconductor bandgap the result is formation of electronic charge carriers, electrons in the conduction band and holes in the valence band, see equation (3.2.1).

$$2h\nu + \text{Semiconductor} \rightarrow 2h^+ + 2e^- \quad (3.2.1)$$

$$2h^+ + H_2O\ (l) \rightarrow \tfrac{1}{2}\ O_2(g) + 2H^+ \quad (3.2.2)$$

$$2H^+ + 2e^- \rightarrow H_2(g) \quad (3.2.3)$$

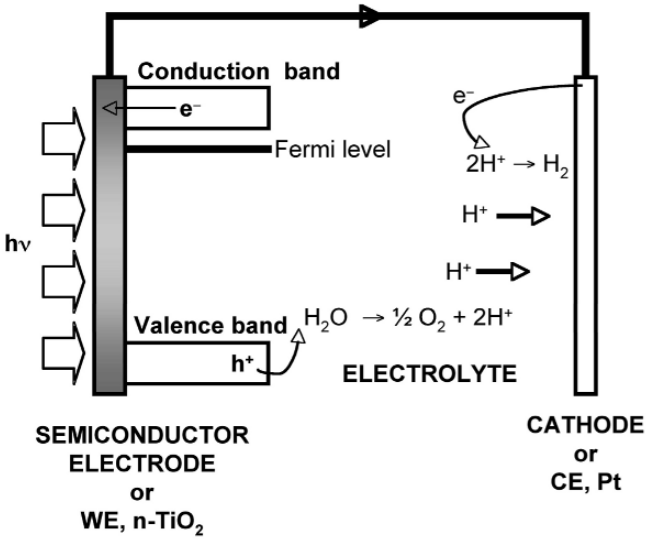

Fig. 3.4b: Illustration of the operating principle of a photoelectrochemical cell producing hydrogen and oxygen during water photoelectrolysis.

At the interface between the photoelectrode and electrolyte, the photogenerated holes h^+ react with water to form oxygen and hydrogen ions H^+. Gaseous oxygen is evolved at the photoelectrode, and the resulting hydrogen ions travel through the aqueous electrolyte (referred to as the internal circuit) to the cathode, equation (3.2.2). At the same time the photogenerated electrons, transferred through the external circuit to the cathode, react with hydrogen ions at the cathode - electrolyte interface reducing the hydrogen ions to gaseous hydrogen, equation (3.2.3).

Under standard conditions water can reversibly electrolyze at a potential of 1.23 V, a value derived from the following relationship;

$$\Delta G^0 = -nF \cdot \Delta E^0 \tag{3.2.4}$$

where ΔG^0 and ΔE^0 are standard Gibbs free energy change and standard electric potential of the reaction. In any redox reaction, the energy released in a reaction due to movement of charged particles gives rise to a potential difference. The maximum potential difference is called the electromotive force (emf or ΔE). The overall reaction of a photoelectrochemical cell, expressed in the following form

$$H_2O + h\nu \rightarrow H_2 + 1/2O_2 \tag{3.2.5}$$

can take place when the energy of the photon absorbed by the working electrode is equal to or larger than the water splitting threshold energy of 1.23 eV. Equation (3.2.5) is an endothermic process and involves a change in the Gibbs free energy, equation (3.2.4), which is the negative value of maximum electric work corresponding to 237.14 kJ/mol or 2.46 eV for equation (3.2.5). Since this is a two-electron redox process electrochemical decomposition of water is possible when the cell emf is equal to or greater than 1.23 V.

3.3 Types of Photoelectrochemical Devices

There are three general types of photoelectrochemical devices using semiconductor electrodes for the conversion of water into hydrogen [17-54].

3.3.1 Photoelectrolysis Cell [26-34]

In this type of cell both electrodes are immersed in the same constant pH solution. An illustrative cell is [27,28]: n-$SrTiO_3$ photoanode|9.5-10 M NaOH electrolyte|Pt cathode. The underlying principle of this cell is production of an internal electric field at the semiconductor-electrolyte interface sufficient to efficiently separate the photogenerated electron-hole pairs. Subsequently holes and electrons are readily available for water oxidation and reduction, respectively, at the anode and cathode. The anode and cathode are commonly physically separated [31-34], but can be combined into a monolithic structure called a photochemical diode [35].

3.3.2 Photo-assisted Electrolysis Cell [36-48]

These cells operate under illumination in combination with a bias, which serves to either drive electrolytic reactions for which the photon energy is insufficient or to increase the rate of chemical energy conversion by reducing electron-hole recombination in the semiconductor bulk. Most commonly an electrical bias is provided to drive the reactions [36-41].

Chemically biased photo-assisted photoelectrolysis cell [42-45]

A chemical bias is achieved by using two different electrolytes placed in two half-cells, with the electrolytes being chosen to reduce the voltage required to cause the chemical splitting. An n-TiO_2 photoanode|4M KOH||4M HCl|Pt-cathode is one example of a chemically biased photoelectrochemical cell [44].

Dye sensitized photoelectrolysis cell [46-48]

This cell involves the absorption of light by dye molecules spread on the surface of the semiconductor, which upon light absorption will inject electrons into the conduction band of the n-type semiconductor from their excited state. The photo-oxidized dye can be used to oxidize water and the complementary redox process can take place at the counter electrode [46,47]. Tandem cells such as these are discussed in Chapter 8.

3.3.3 Photovoltaic Electrolysis Cell [48-54]

This cell employs a solid state photovoltaic to generate electricity that is then passed to a commercial-type water electrolyzer (see Chapter 2). An alternative system involves the semiconductor photovoltaic cell configured as a monolithic structure and immersed directly in the aqueous solution, see Chapter 8; this cell involves a solid-state p-n or schottky junction to produce the required internal electric field for efficient charge separation and the production of a photovoltage sufficient to decompose water [49-51].

3.4 Photoelectrolysis Principles

Photoelectrolysis is generally carried out in cells having similar configuration as electrolysis cells (discussed in Chapter 2) with at least one of the two electrodes comprised of a semiconductor material. Upon exposure to sunlight the semiconductor electrode, called photoelectrode, immersed in an aqueous electrolyte solution generates, in an ideal case, enough electrical energy to drive the oxygen and hydrogen evolution reactions respectively at the interfaces of anode and cathode within the electrolyte. A necessary condition for such a spontaneous water splitting process upon illumination is that the semiconductor conduction band edge should lie at a position more negative (NHE as reference) relative to the reduction potential of water while the valence band edge more positive compared to the oxidation potential. However, in many material-electrolyte systems the conduction band edge is located close to or more positive relative to the reduction potential of water. Such a situation in the case of titania and an aqueous electrolyte of pH=1 is depicted in **Fig. 3.5**. In most cases the photovoltage developed between the electrodes is less than 1.23V, the minimum voltage required for water splitting. For example, a widely studied photoanode material rutile TiO_2 [36-40,42-44], 3.0 eV bandgap, generates photovoltages of only 0.7-0.9 V under solar light illumination. Hence water splitting can be effectively performed only with the assistance of an external electrical bias or internal chemical bias (by creating anode and cathode compartments with different hydrogen ion concentrations).

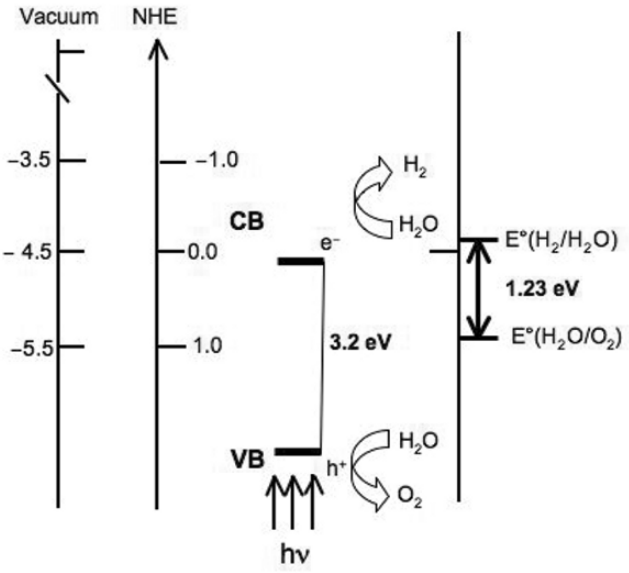

Fig. 3.5: Band position of anatase TiO_2, bandgap = 3.2 eV, in the presence of a pH = 1 aqueous electrolyte. The energy scale is indicated in electron volts (eV) using either normal hydrogen electrode (NHE) or vacuum level as reference showing the condition for water splitting.

For meaningful photoelectrochemical decomposition of water to occur three essential requirements must be met [11,17-20,55-65]. First, the conduction and valence band edges of the semiconductor materials must overlap, the energy levels of the hydrogen and oxygen reduction reactions, **see Fig. 3.5**. Second, the semiconductor system must be stable under photoelectrolysis conditions. Third, charge transfer from the surface of the semiconductor must be fast enough to prevent corrosion and also reduce energy losses due to overvoltage or overpotential.

3.4.1 Energy Levels in Semiconductors and Electrolytes

The electronic structure of the semiconductor electrodes is usually described in terms of energy bands that can effectively be considered a continuum of energy levels due to the small difference in energy between adjacent molecular orbitals [66,67]. The highest energy band comprised of occupied molecular orbitals is called the

valence band, with its upper energy level denoted as E_{VB}. The lowest energy band comprised of unoccupied molecular orbitals, or empty energy states, is called the conduction band with its lower edge denoted as E_{CB}. The difference in energy between the upper edge of valence band and lower edge of the conduction band is the bandgap energy E_{BG}. Electrons can be thermally or photochemically excited from the valence band to the conduction band with the transfer of an electron, e^-, leaving a positively charged vacancy in the valence band which is referred to as a hole, h^+. Holes are considered mobile since holes are created by the migration of electrons. The Fermi energy level is defined as the energy level at which the probability of occupation by an electron is one-half. The Fermi energy level can be calculated by the following formula

$$E_F = \frac{1}{2}\left(E_{VB} + E_{CB}\right) + \frac{1}{2}\left(kT \ln \frac{N_{VB}^*}{N_{CB}^*}\right) \tag{3.4.1}$$

Where E_{CB} and E_{VB} are, respectively, the energy levels of the conduction and valence band edges, k (1.38×10^{-23} J/K) is the Boltzmann constant, and T (Kelvin scale, K) is the temperature. N_{VB}^* and N_{CB}^* are the effective density of (energy) states function in the valence and conduction bands

$$\mathrm{N}_{\mathrm{VB}}^* = 2\left[\frac{2\pi m_h^* kT}{h^2}\right]^{3/2} \tag{3.4.2}$$

$$\mathrm{N}_{\mathrm{CB}}^* = 2\left[\frac{2\pi m_e^* kT}{h^2}\right]^{3/2} \tag{3.4.3}$$

in which h is Plank's constant, and m_h^* and m_e^* are, respectively, the effective masses of holes and electrons that takes into account their ability to move through the atomic lattice [67].

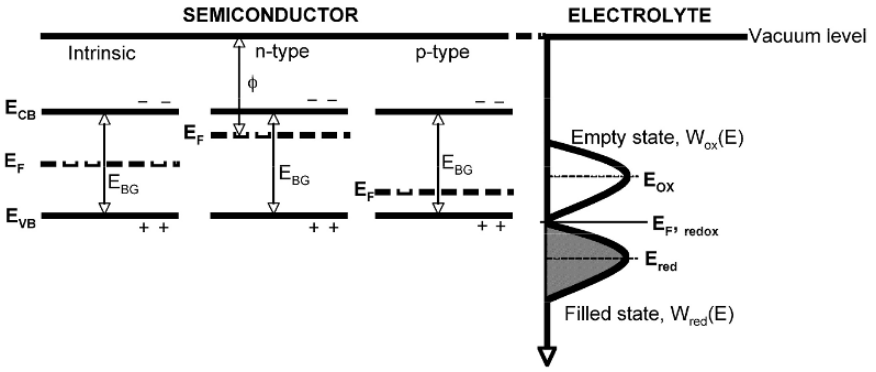

Fig. 3.6: A schematic representation of semiconductor energy band levels and energy distribution of the electrolyte redox system.

As shown in **Fig. 3.6**, for intrinsic (undoped) semiconductors the number of holes equals the number of electrons and the Fermi energy level E_F lies in the middle of the band gap. Impurity doped semiconductors in which the majority charge carriers are electrons and holes, respectively, are referred to as n-type and p-type semiconductors. For n-type semiconductors the Fermi level lies just below the conduction band, whereas for p-type semiconductors it lies just above the valence band. In an intrinsic semiconductor the equilibrium electron and hole concentrations, n_0 and p_0 respectively, in the conduction and valence bands are given by:

$$n_0 = N_{CB}^{*} \cdot e^{\left(-\frac{E_{CB}-E_F}{kT}\right)} \tag{3.4.4}$$

$$p_0 = N_{VB}^{*} \cdot e^{\left(-\frac{E_F-E_{VB}}{kT}\right)} \tag{3.4.5}$$

Multiplying equations (3.4.4) and (3.4.5) an equilibrium concentration can be expressed as [20]:

$$n_0 p_0 = N_{CB}^{*} N_{VB}^{*} \cdot e^{\left(-\frac{E_{CB}-E_{VB}}{kT}\right)} = n_i^2 \tag{3.4.6}$$

n_i^2 is the intrinsic carrier concentration which exponentially decreases with increasing bandgap. Electron and hole concentrations

can also be obtained as a function of donor and acceptor impurity concentrations. At equilibrium

$$n_0 = \frac{N_d}{2} + \sqrt{\left(\frac{N_d}{2}\right)^2 + n_i^2} \tag{3.4.7}$$

$$p_0 = \frac{N_a}{2} + \sqrt{\left(\frac{N_a}{2}\right)^2 + n_i^2} \tag{3.4.8}$$

From equations (3.4.4) and (3.4.5) one can determine the energy difference between the energy band edges and the Fermi level [67].

$$E_{CB} - E_{F,n} = kT \ln \frac{N_{CB}^*}{n} \tag{3.4.9}$$

$$E_{F,p} - E_{VB} = kT \ln \frac{N_{VB}^*}{p} \tag{3.4.10}$$

For an n-type semiconductor, if the donor impurity concentration is much greater than the intrinsic carrier concentration, $N_d >>> n_i$, then $n_0 \approx N_d$. Equation (3.4.9) can then be written as

$$E_F = E_{CB} - kT \ln \frac{N_{CB}^*}{N_d} \tag{3.4.11}$$

From equation (3.4.11) we see that the energy gap between the conduction band edge and the Fermi energy level is a logarithmic function of donor concentration. As the donor concentration increases so does the electron concentration in the conduction band, with the Fermi level energy moving closer to the conduction band edge.

Similarly, one can derive an equation for a p-type semiconductor, where the distance between the Fermi energy level and the valence band is a logarithmic function of acceptor impurity concentration. As the acceptor impurity increases so too does the hole concentration in valence band, with the Fermi level moving closer to the valence band.

$$E_F = E_{VB} + kT \ln \frac{N_{VB}^*}{N_a} \tag{3.4.12}$$

The Fermi energies are related to the electrochemical potential of electrons and holes, which are usually given with respect to a reference electrode, commonly the normal hydrogen electrode (NHE) or Standard Calomel electrode (SCE). Considering a simple redox couple, to correlate energy positions in relation to the electrolyte the electrode potential (V) must be converted into the free energy of electrons at the same electrostatic potential. The electrochemical potential of electrons in a redox system is equivalent to the Fermi level, $E_{F,redox}$ on an absolute scale [68]. Hence the electrochemical potential of a redox system, usually given with respect to NHE, is described by the following relationship:

$$E_{F,redox} = -eV_{redox} + const_{ref} \tag{3.4.13}$$

Where V_{redox} is the redox potential *vs* NHE and $const_{ref}$ is the free energy of the electrons in the reference electrode with respect to vacuum level. Since the electrochemical scale is arbitrarily based on a reference electrode the connection between these two electrodes is given by a work function (ϕ) for the removal of an electron from the Fermi level of the reference electrode to the vacuum level. For NHE, the constant has a value between –4.5 to –4.7 eV. Thus equation (3.4.13) can be written as

$$E_{F,redox} = -4.5eV - eV_{redox} \tag{3.4.14}$$

with respect to vacuum level [69,70].

Figure 3.6 shows the various relationships between the energy levels of solids and liquids. In electrolytes three energy levels exist, $E_{F,\ redox}$, E_{ox} and E_{red}. The energy levels of a redox couple in an electrolyte is controlled by the ionization energy of the reduced species E_{red}, and the electron affinity of the oxidized species E_{ox} in solution in their most probable state of solvation; due to varying interaction with the surrounding electrolyte, a considerable

fluctuation in their energy levels occurs. The standard redox potential is an average of the ionization energy and the electron affinity. This energy level is attained with equal probability by fluctuations of the ionization energy of the reduced, and the electron affinity of the oxidized, species. As illustrated on the right side of **Fig. 3.6,** the Gaussian distribution of E_{ox} and E_{red} is a consequence of these energy level fluctuations of redox species in solution; for each single redox species a probability distribution of energy states can be described as follows;

$$W_{ox}\left(E\right) = e^{\left(-\frac{\left(E_{ox}-E\right)^2}{4kT\lambda}\right)} \tag{3.4.15}$$

$$W_{red}\left(E\right) = e^{\left(-\frac{\left(E_{red}-E\right)^2}{4kT\lambda}\right)} \tag{3.4.16}$$

The most probable energy levels E_{ox} and E_{red} are connected with the standard redox potential or by the standard redox Fermi level by the following symmetrical relation:

$$E_{red} = E_{F,redox} - \lambda \tag{3.4.17}$$

$$E_{ox} = E_{F,redox} + \lambda \tag{3.4.18}$$

where λ is the reorganization energy, defined as the energy needed to bring the solvation shell of one redox species from its most probable state into the most probable solvation structure of its redox counter part. The width of the distribution function in equations (3.4.15) and (3.4.16) is controlled by the reorganization energy λ.

3.4.2 The Semiconductor-Electrolyte Interface

Band bending at the interface

Helmholtz [71] first described the interfacial behavior of a metal and electrolyte as a capacitor, or so-called “electrical double layer,” with the excess surface charge on the metallic electrode remaining separated from the ionic counter charge in the electrolyte by the thickness of the solvation shell. Gouy and Chapmen subsequently

developed a diffuse ionic double layer model, in which the potential at the surface decreases exponentially due to chemisorbed counter ions from the electrolyte solution. Thus the movement of the ionic counter charges of an electrolyte, near the surface of a metal electrode, makes them lose part of their solvation shell [72,73].

Unlike metals, semiconductors do not possess high conductivity hence diffuse ionic double layer models can be used to describe the interfacial properties between a semiconductor electrode and a liquid [11,17-20,55-65,74-77]. Three different situations are depicted for n-type, **Fig. 3.7 (a-c)**, and p-type, **Fig. 3.7 (d-f)**, semiconductors. When a semiconductor photoelectrode is brought into contact with an electrolyte solution the excess charge does not lie on the surface, but rather extends into the electrode for approximately 1 μm; this region is called the space charge region (or space charge layer), and has an associated electric field. Charge transfer from the semiconductor to electrolyte leads to the formation of surface charge, which is then compensated by a charge of opposite sign induced in the electrolyte within a localized layer known as the Helmholtz layer. The Helmholtz layer is formed by oriented water molecule dipoles and adsorbed electrolyte ions at the electrode surface. The unusual charge distribution results in band bending at the semiconductor-electrolyte interface. For an electrolyte-immersed n-type semiconductor a depletion layer forms where the region is depleted of electrons, leaving a net positive charge balance behind that is compensated for at the interface by negative counter ions from the electrolyte, **Fig. 3.7(a)**. Similarly, an accumulation layer forms when the negative excess charge (electrons) of a semiconductor accumulates at the interface, which is compensated by the positive ions of an electrolyte, **Fig. 3.7(b)**. **Fig. 3.7(c)** shows an interface where no net excess charge on a semiconductor is observed, hence the bands are flat, reflecting the potential of zero charge for photoelectrode; this potential is called the flat band potential, V_{FB}.

For p-type semiconductors, an accumulation layer forms when excess positive charge (holes) accumulate at the interface, which is compensated by negative ions of an electrolyte, **Fig. 3.7(d)**. Similarly, a depletion layer forms when the region containing negative charge is depleted of holes, and thus positive counter ions

from the electrolyte compensates charge at the interface, **Fig. 3.7(e)**. When no net excess charge is observed on an interface there is no band bending, reflecting the zero charge potential of the photoelectrode, **Fig. 3.7(f)**; this potential is called the flat band potential, V_{FB}.

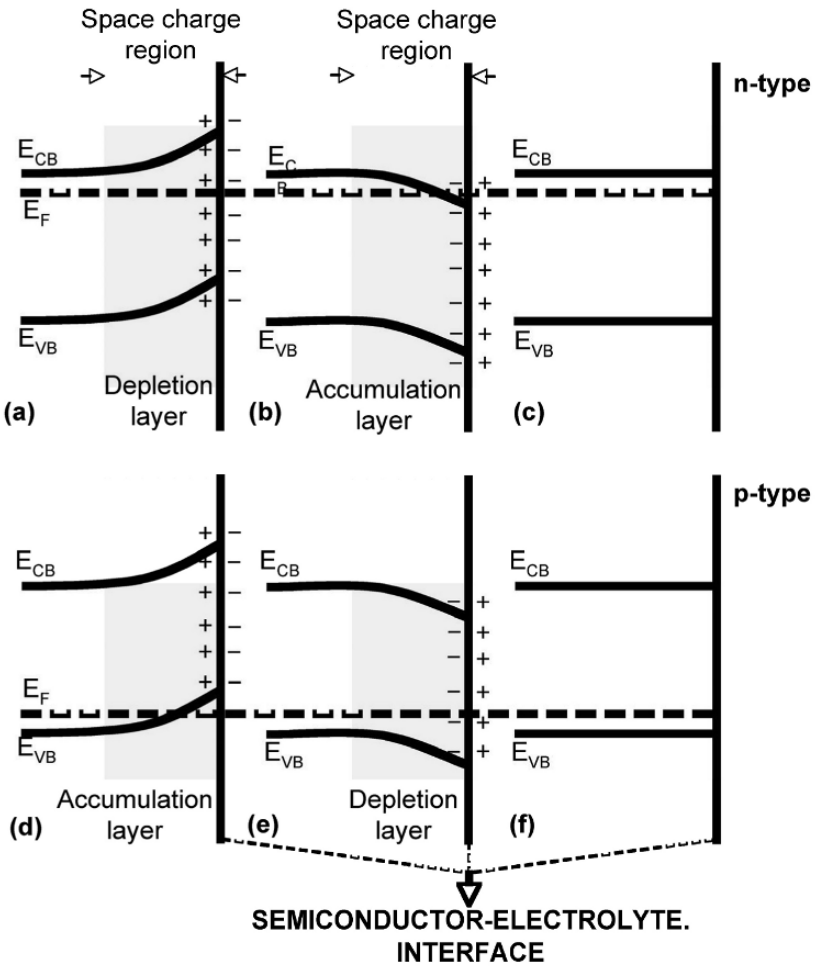

Fig. 3.7: Band bending at semiconductor-electrolyte interface.

Equilibrium between the two phases at a semiconductor-electrolyte interface, solid and liquid, can only be achieved if their electrochemical potential is the same, that is:

$$E_F = E_{F,\,redox} \tag{3.4.19}$$

The electrochemical potential of the solution and semiconductor, see **Fig. 3.6**, are determined by the standard redox potential of the electrolyte solution (or its equivalent the standard redox Fermi level, $E_{F,redox}$), and the semiconductor Fermi energy level. If these two levels do not lie at the same energy then movement of charge across the semiconductor - solution interface continues until the two phases equilibrate with a corresponding energy band bending, see **Fig. 3.8**.

For an n-type semiconductor electrode the Fermi level is typically higher than the redox potential of the electrolyte, hence electrons move from the electrode to electrolyte solution leaving positive charge behind in the space charge region reflected by upward band bending. Withdrawal of the semiconductor majority charge carriers from the space charge region ensures the formation of a depletion layer in this region, **Fig. 3.7(a)** and **Fig. 3.8(a)**. For a p-type semiconductor the Fermi level lies lower than the redox potential, therefore electrons move from solution to the semiconductor electrode to attain equilibrium. In this process, negative charge in the space charge region causes downward band bending, with the removal of holes from the space charge region ensuring formation of a depletion layer, **Fig. 3.7(e)** and **Fig. 3.8(b)**.

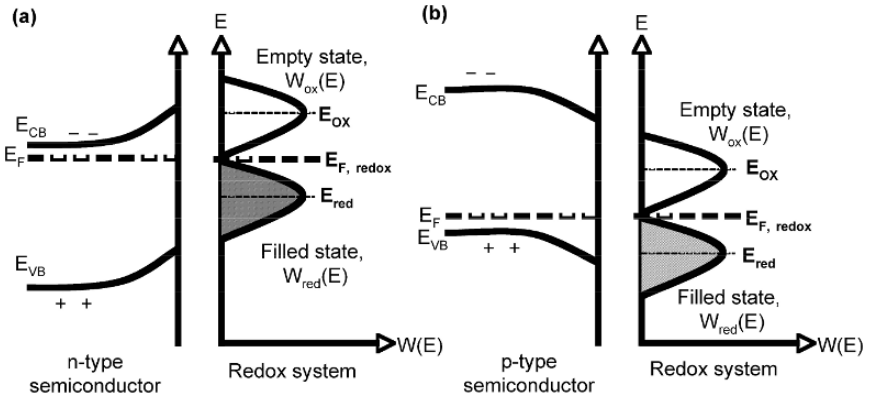

Fig. 3.8: Electron energy distribution at the contact between a semiconductor and a redox electrolyte for two different redox systems at equilibrium. **(a)** n-type semiconductor, and **(b)** p-type semiconductor.

Potential Distribution Across the Interface

Let us consider an n-type semiconductor in equilibrium with a redox couple, $E_F = E_{F,redox}$, with formation of the space charge layer leading to band bending as shown in **Fig. 3.9(a)**. A potential (V_E) is established between the working semiconductor electrode, under potentiostatic control, and the reference electrode. In the case of an ideally polarizable interface, i.e. when there is no exchange of charge with the electrolyte, the potential of the bulk semiconductor matches the potential of the redox couple at the reference electrode, **Fig. 3.9(b)**. This indicates that the difference in potential between the semiconductor working electrode and the reference electrode is dependent on the charge concentration in the space charge region.

At a semiconductor-electrolyte interface, if there is no specific interaction between the charge species and the surface an electrical double layer will form with a diffuse space-charge region on the semiconductor side and a plate-like counter ionic charge on the electrolyte side resulting in a potential difference ϕ across the interface. The total potential difference across the interface can be given by

$$V_E = \phi_H + \phi_{SC} + \phi_G + C \tag{3.4.20}$$

where V_E is the electrode potential measured in relation to the reference electrode. ϕ_H is the interfacial difference potential between the solid and the liquid phases, commonly called the Helmhotz potential; ϕ_{SC} is the potential difference developed across the space charge layer; constant C depends on the nature of reference electrode. There also exists a diffuse double layer (Gouy region, ϕ_G) that can be neglected under sufficiently high redox electrolyte concentration.

A representative potential distribution across the interface is shown in **Fig. 3.9(c)**, taking the potential of the bulk solution as zero. The potential difference across the space charge region (ϕ_{SC}) occurs over a larger distance than that of the Helmholtz layer (ϕ_H). For an n-type semiconductor, ϕ_{SC} results from the excess positive charge of ionized donors in the bulk of the space charge region within the

solid, and ϕ_H is due to the accumulation (~1 nm thick layer) of negative ions in the electrolyte solution from the solid surface, **Fig. 3.9(d)**.

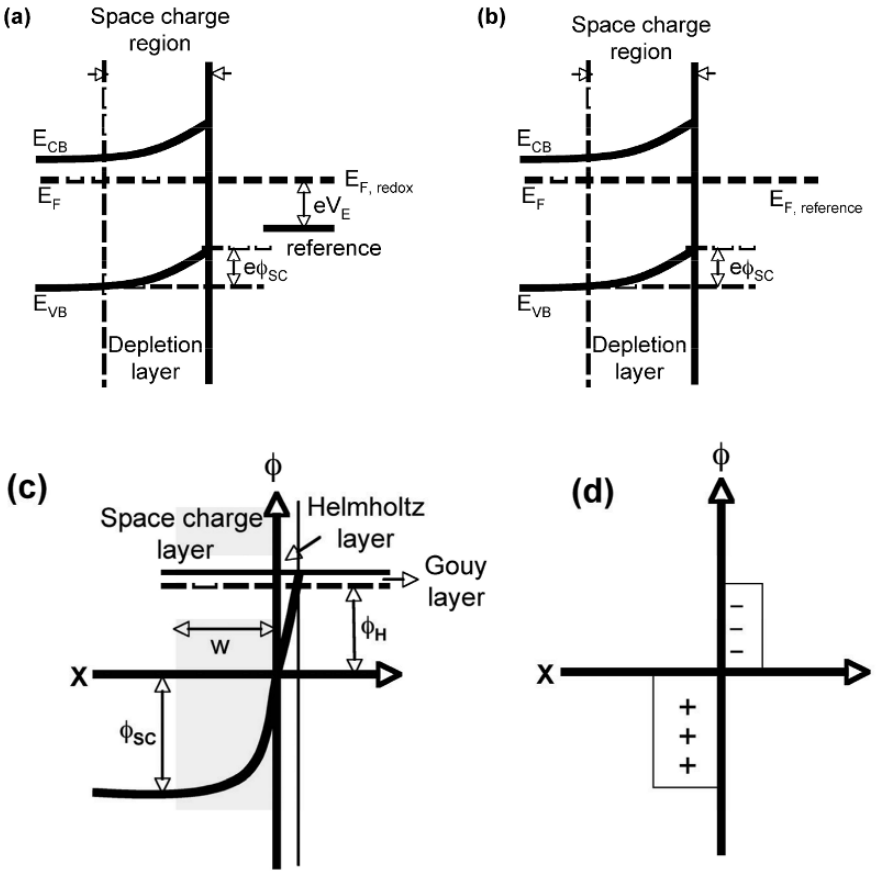

Fig. 3.9: Energy diagram of the semiconductor-electrolyte interface under equilibrium. **(a)** The Fermi level E_F is equal to redox potential energy, $E_{F,\ redox}$ **(b)** The Fermi level, E_F is equal to reference electrode energy, $E_{reference}$. **(c)** Potential distribution. **(d)** Charge across the interface.

For a p-type semiconductor, ϕ_{SC} results from the excess negative charge associated with the ionized acceptors in the space charge region of the solid, and ϕ_H is due to the accumulation of a positive ion layer (~1 nm thick, from the solid surface) in the

electrolyte solution. A Helmholtz layer a few Angstroms thick is formed from oriented solvent molecule dipoles and electrolyte ions adsorbed at the semiconductor electrode surface, while the space charge layer is formed by the distribution of the semiconductor counter charges such as electrons, holes, ionized donors and ionized acceptor states over a finite distance below the semiconductor. The amount of chemisorbed ionic charge at the surface depends mainly on the electrolyte composition, and to a much lesser degree the excess charge on the semiconductor. Since the charge in both regions is equal but of opposite sign, comparison of the capacitance of the space charge region (C_{sc}) with the Helmholtz capacitance (C_H) shows that C_{sc} usually much smaller. Under these conditions ϕ_H remains essentially constant, with changes in the applied potential between the semiconductor electrode and reference electrode appearing in ϕ_{SC} so that:

$$V_E = \phi_{SC} + V_{FB} \tag{3.4.21}$$

V_{FB} is the flat band potential, and at this potential the surface concentration of charge is equal to that of the bulk. The effect of applied potential on the band edges of bulk n-type and p-type semiconductors are shown in **Fig. 3.7**. When the applied potential is more positive than the flat band potential ($V_E > V_{FB}$) a depletion layer forms in an n-type semiconductor, while for a p-type semiconductor the surface concentration of electrons decreases creating an accumulation layer of holes, and the bending of the bands at the surface to higher energies. Similarly, when the applied potential is more negative than the flat band potential ($V_E < V_{FB}$) an accumulation layer forms in the n-type semiconductor due to an excess of electrons in space charge layer, while for a p-type semiconductor the additional electrons produce a depletion layer, bending the energy bands at the surface downward to lower energies.

The electronic charge distribution in a semiconductor varies with applied electrode potential (V_E), which in turn determines the differential capacitance at the interface [11,78]. Relating charge density and electric field, the capacitance of a space charge (or depletion) region can be quantitatively derived. For an n-type semiconductor Poissons' equation can be written:

$$\frac{\partial^2 \phi}{\partial x^2} = \frac{eN_D}{\varepsilon\varepsilon_0} \tag{3.4.22}$$

where e is electronic charge, N_D is the electron donor concentration, ε_0 is the permittivity of space, and ε is the relative dielectric constant of the medium. Assuming the electric field $\frac{d\phi}{dx}$ is zero at x_0 ($0 \le x \le w$) integrating equation (3.4.22) across the length of the space charge layer *w* we find:

$$\phi_{SC} = \frac{eN_D}{2\varepsilon\varepsilon_0} \cdot w^2 \tag{3.4.23}$$

An electric field is generated in the depletion region due to ionized donors and a gradient in electron concentration. From Gauss's law we find

$$\left(\frac{d\phi}{dx}\right)_{\phi \to \phi_{SC}} = \frac{Q_{SC}}{\varepsilon\varepsilon_0 A} \tag{3.4.24}$$

where A is the electrode area. The total charge moving through the depletion region is

$$Q_{sc} = e \cdot N_D \cdot A \cdot w \tag{3.4.25}$$

The capacitance of the space charge region is given by

$$C_{SC} = \frac{dQ}{d\phi} = e \cdot N_D \cdot A \cdot \frac{dw}{d\phi} \tag{3.4.26}$$

Using equations (3.4.23)-(3.4.26), for $\phi \to \phi_{sc}$, two equations can be derived.

$$C_{SC} = \frac{\varepsilon\varepsilon_0 A}{w} \tag{3.4.27}$$

$$\frac{1}{C_{SC}^2} = \left(\frac{2}{e\varepsilon\varepsilon_0 N_D} \right) \left(\phi_{SC} - \frac{kT}{e} \right) \tag{3.4.28}$$

Equation (3.4.28) is commonly known as Mott-Schottky equation.

The space charge layer capacitance is inversely proportional to the width of the depletion layer *w*. As the width of the depletion layer approaches zero the capacitance approaches infinity, hence $\frac{1}{C_{SC}^2}$ will be zero at the flat band potential. Using equation (3.4.21) to modify equation (3.4.28) the Mott-Schottky relation can be described as:

$$\frac{1}{C_{SC}^2} = \left(\frac{2}{e\varepsilon\varepsilon_0 N_D} \right) \left((V_E - V_{FB}) - \frac{kT}{e} \right) \tag{3.4.29}$$

Donor density can be calculated from the slope of $\frac{1}{C_{SC}^2}$ *vs* applied potential, and the flat band potential determined by extrapolation to $\frac{1}{C_{SC}^2} = 0$. **Fig. 3.10** represents the Mott-Schottky plot for both n-type and p-type GaAs in an ambient temperature molten salt electrolyte made up of $AlCl_3$/n-butylpyridinium chloride [79]. The capacitance dependence on applied potential is an important means of characterizing a semiconductor-electrolyte interface [80-84]. The flat band potential is the difference between the Fermi level of the semiconductor and the Fermi level of the reference electrode. Using equations (3.4.11) and (3.4.12) one can then determine the conduction and valence band edges of the semiconductor with reference to vacuum energy level, and thus the bandgap of the semiconductor.

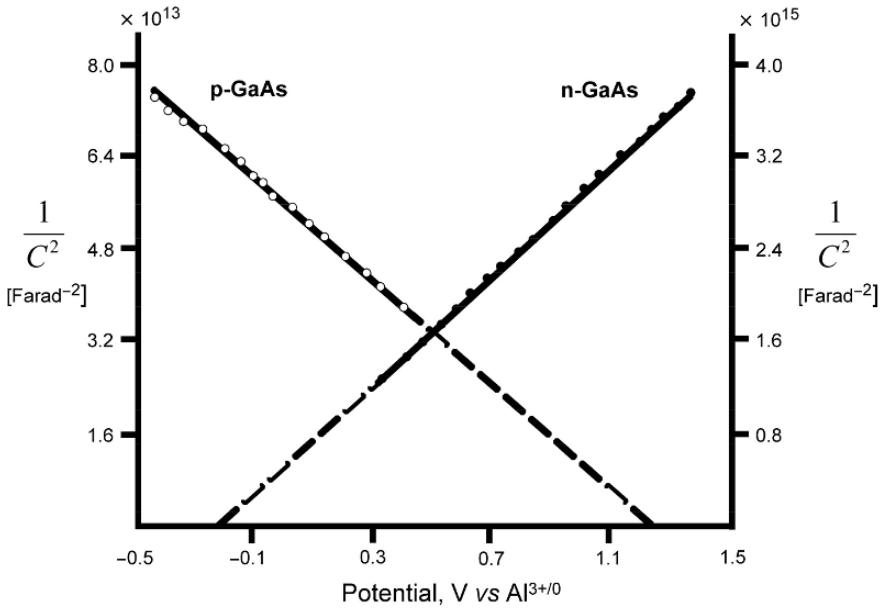

Fig. 3.10: Mott-Schottky plot for n-type and p-type semiconductor of GaAs in $AlCl_3$/n-butylpyridinium chloride molten-salt electrolyte [79].

The acidic or basic character of a semiconductor surface gives rise to interaction with H^+ or OH^- ions of an aqueous electrolyte:

$$M{-}O + H_2O \leftrightarrow HO{-}M^+ + OH^- \qquad \textbf{(A)}$$
$$M{-}O + H_2O \leftrightarrow M{-}(OH)_2 \leftrightarrow HO{-}M{-}O^- + H^+ \qquad \textbf{(B)}$$

where M stands for metal ions. Since the charge balance across the solid-liquid interface is potential dependent, the Helmholtz double layer varies with the change in the H^+ or OH^- concentrations, that is to say the *pH* of the electrolyte. This behavior can be expressed:

$$\phi_H = const. + 0.059pH \qquad (3.4.30)$$

In many cases the flat band potential, and hence the semiconductor band edge varies with the pH of the aqueous electrolyte solution, as illustrated in **Fig. 3.11**.

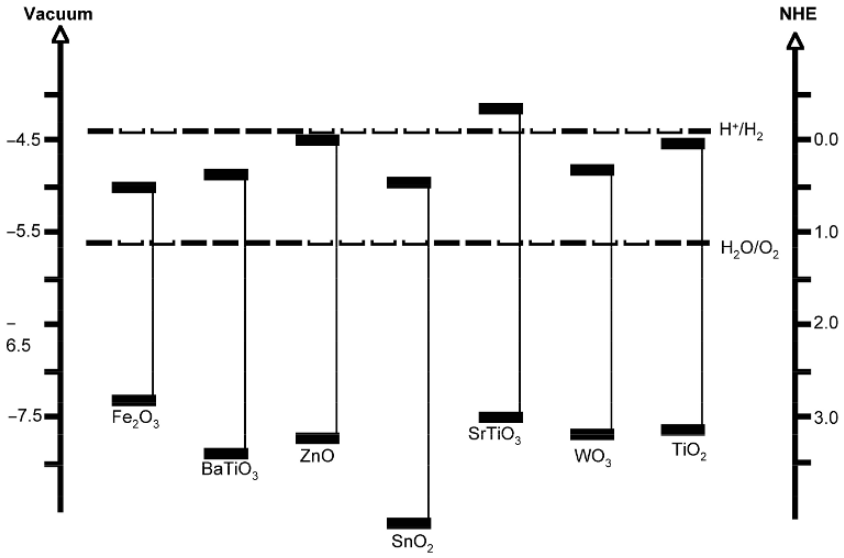

Fig. 3.11a: Band edge positions of several oxide semiconductors in contact with a pH 1 aqueous electrolyte.

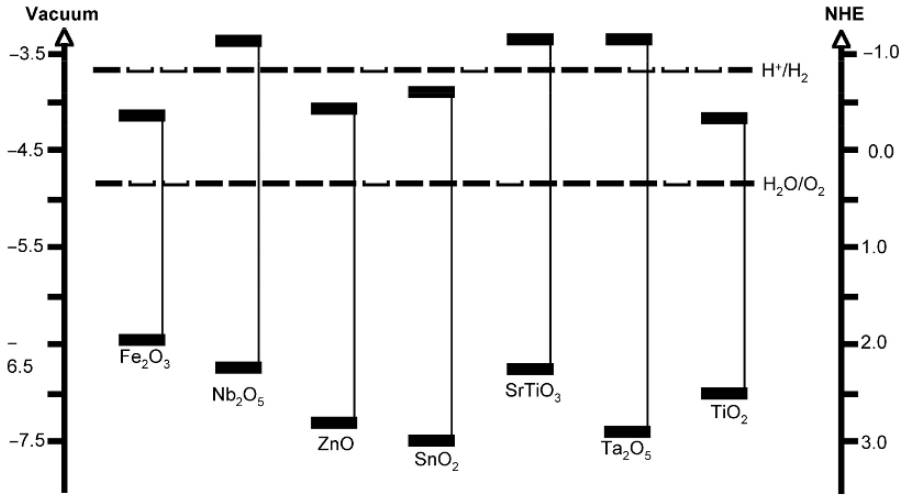

Fig. 3.11b: Band edge positions of several oxide semiconductors in contact with a pH 7 aqueous electrolyte.

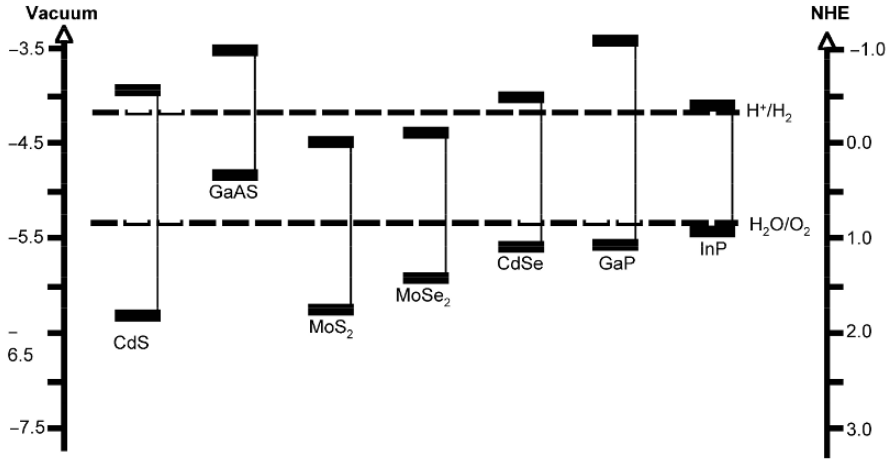

Fig. 3.11c: Band edge positions of several non-oxide semiconductors in contact with a pH 13 aqueous electrolyte.

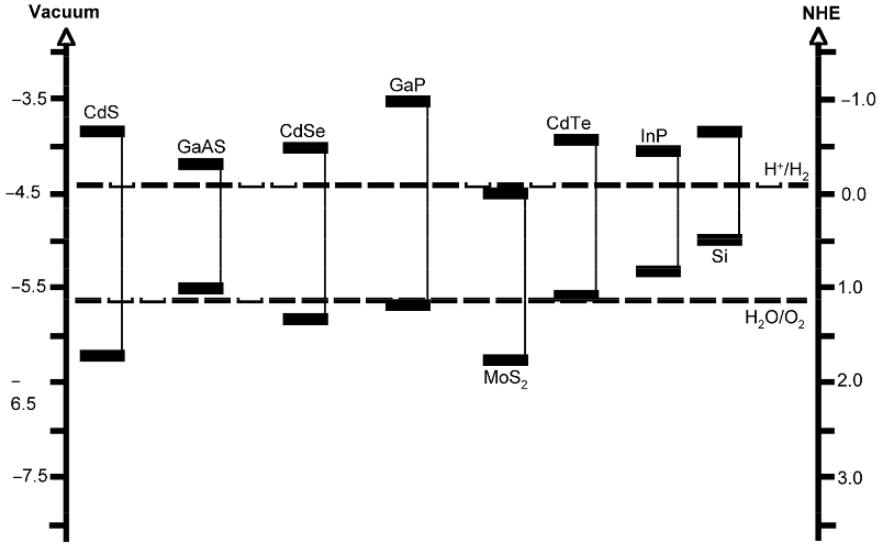

Fig. 3.11d: Band edge positions of several non-oxide semiconductors in contact with a pH 1 aqueous electrolyte

Charge Transfer Processes at the Interface

The Fermi level of a liquid immersed metal electrode largely defines its electrochemical potential; as long as one remains in equilibrium with the empty acceptor state or with the filled donor state of the solution redox species electron transfer occurs in an energy range close to the Fermi level [85,86]. In the case of a metal electrode the density of states at the Fermi energy level, and the corresponding charge carrier concentration, is very high therefore the rate constant at the metal electrode/solution interface can be easily controlled through the potential difference across the Helmholtz layer. Modulation of this potential difference readily enables characterization of the electron-transfer kinetics at the metal electrode/solution interface.

In contrast to metal electrodes, for a semiconductor-electrolyte interface most of the potential drop is located in the semiconductor making it difficult to study interfacial processes using potential perturbation techniques [11,20,55,58,60-65,75-78]. H. Gerischer [76] proposed a model in which electrons and holes are considered as individual interfacial reactants. Distinct and preferential electron transfer reactions involve either the conduction band or valence band as dependent on the nature of the redox reactants of the electrolyte, with specific properties dependent upon the energy state location.

The energy level of an electrolyte redox couple is governed by the ionization potential of the reduced species and the electron affinity of the oxidized species. As shown in equations (3.4.17)-(3.4.19) the Fermi level at a semiconductor surface adjusts itself to the position of the redox Fermi level by a factor λ due to the appropriate charging of the electric double layer, thus an equilibrium between the two can be achieved. Unless there is a considerable change in the Helmholtz layer potential (ϕ_H) due to variation of the electrical double layer charge, the semiconductor band edge energies do not change with respect to the redox couple energy level. Rather it is the electron and hole surface concentrations that vary with the double layer charge. For a given applied voltage, equilibrium between a semiconductor and an electrolyte is established by the adjustment of electron and hole concentrations.

Let us consider an n-type semiconductor in equilibrium with three different redox couples. In **Fig. 3.12(a)** the Fermi level of the redox couple is close to conduction band edge forming an accumulation layer at equilibrium; in this case electrons are available at the semiconductor surface showing a high rate of electron transfer between the redox system and the conduction band. As shown in **Fig. 3.12(b)** the semiconductor has formed a depletion layer. For this case electrons are not available at the surface for transitions to the oxidized species, while electrons in the reduced species cannot reach the conduction band energy; the result is no electron exchange. **Fig. 3.12(c)** shows an even higher barrier height for electrons that precludes electron exchange with the conduction band. Since the Fermi level of the redox couple overlaps with the valence band it is clear that reduction and oxidation of this system are valence band processes better described by the exchange of (valence band) holes across the interface. Formation of an inversion energy barrier layer between the bulk electrons and holes on or near the surface retards the hole exchange process at the electrode surface.

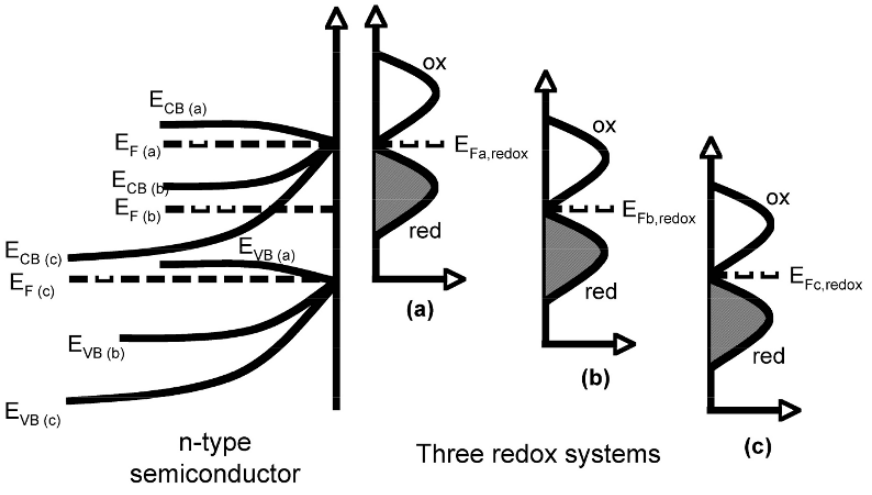

Fig. 3.12: Three different redox systems in equilibrium with an n-type semiconductor: **(a)** exchange of electrons with conduction band, **(b)** no or negligible electron exchange, and **(c)** exchange of electrons with valence band.

With reference to the Gerischer model [11,76,77], the charge transfer reaction of a semiconductor electrode in contact with a

redox electrolyte is generally considered a bimodal reaction taking into account the concentration of redox ions in solution and the concentration of surface electrons/holes in the solid. The rate of electron transfer in the conduction band J_C is based on kinetics that considers both electrons and holes as reactants. The current due to conduction band transfer processes can be expressed as:

$$\frac{J_C}{J_{C,0}} = \left\{ \frac{[C_{red}]}{[C_{red,0}]} - \frac{n_s}{n_{s,0}} \cdot \frac{[C_{ox}]}{[C_{ox,0}]} \right\} \tag{3.4.31}$$

where C_{red}, C_{ox}, and n_s represent, respectively, concentrations of the reduced component, concentration of the oxidized component, and surface concentration of electrons. $C_{red,0}$, $C_{ox,0}$, and $n_{s,0}$ are the same parameters at equilibrium. $J_{C,0}$ is the exchange current density in the conduction band at equilibrium. Note that the exchange current density is a function of the electrode material(s) and the electroactive specie(s) in solution that at equilibrium are described in the general form:

$$J_{C,0} = e \cdot n_{s,0} \cdot K_{ET} \cdot [A] \tag{3.4.32}$$

where e denotes electronic charge, K_{ET} is the rate constant for electron transfer from the conduction band to the redox acceptor in solution, and A the redox acceptor concentration. The units of the rate constant are $cm^4 \bullet s^{-1}$ due to the second-order kinetics.

From equation (3.4.31), if the ratio $n_s/n_{s,0}$ is unity there will be no net current flow across the interface; this condition is depicted in **Fig. 3.13(a)** for an n-type semiconductor. Under this equilibrium state surface electrons can undergo isoenergetic electron transfers to the redox species due to a built-in potential, equal to the difference of potential between E_{CB} and E_{redox}. Equilibrium can be perturbed, with a resulting observable transient current flow, by varying the concentrations of the redox species. The surface electron concentration n_s is related to the bulk concentration n_0 by the potential difference of the space charge layer as follows:

$$n_s = n_0 \cdot e^{\frac{e\phi_{SC}}{kT}} \tag{3.4.33}$$

The rate of forward electron transfer is equal to the rate of back electron transfer under this equilibrium condition, with no applied bias on the electrodes.

As shown in **Fig. 3.13(b)** and **3.13(c)** when ratio $n_s/n_{s,0}$ is less than or greater than 1 the system is in non-equilibrium resulting in a net current, with the electron transfer kinetics at the semiconductor-electrolyte interface largely determined by changes in the electron surface concentration and the application of a bias potential. Under reverse bias voltage, $V_{E1} > 0$ and $n_{s,0} > n_s$ as illustrated in **Fig. 3.13(b)**, anodic current will flow across the interface enabling oxidized species to convert to reduced species (reduction process). Similarly, under forward bias, $V_{E2} < 0$ and $n_s > n_{s,0}$ as illustrated in **Fig. 3.13(c)**, a net cathodic current will flow.

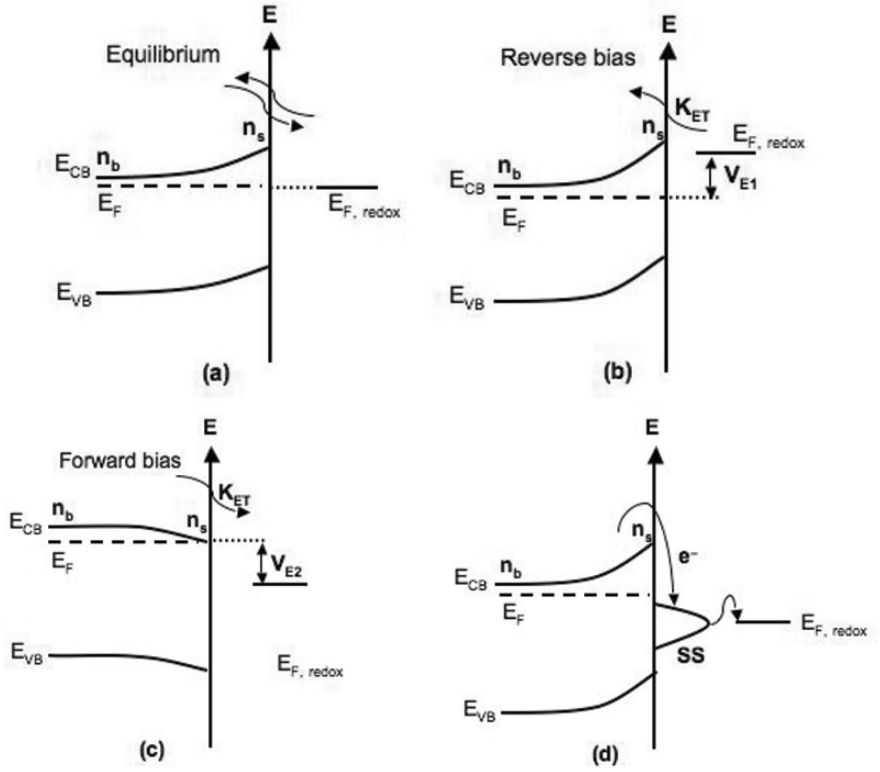

Fig. 3.13: Semiconductor-electrolyte interface **(a)** at equilibrium, **(b)** under reverse bias **(c)** under forward bias. Arrows denote direction of current flow [reduction reaction; ox + $e^- \rightarrow$ red]. **(d)** Electron transfer mediated through surface states.

For an interface described by a constant Helmholtz potential ϕ_H, there is no electron exchange between the semiconductor and redox electrolyte solution. The result is that $dV = d\phi_{SC}$, and for a non-equilibrium system one can obtain the current-voltage relation:

$$J_C = J_{C,0}\left[1 - e^{\frac{e(V_E - V_0)}{kT}}\right] \tag{3.4.34}$$

($V_E - V_0$) is the overpotential, the potential required to initiate reactions at the electrode surface, the difference between the equilibrium potential V_0 (no current flowing) and operating potential V_E (current flowing). The above kinetics indicate that the rate of electron transfer from the n-type semiconductor to the redox system depends on the surface electron concentration, while electron injection from the redox system into the conduction band is constant independent of applied potential [11,76,77]. If the Helmholtz layer potential ϕ_H varies across the interface the description of electron transfer becomes considerably more complicated requiring a charge transfer coefficient in equation (3.4.34).

For hole transfer and hole injection between a p-type semiconductor and a redox system the corresponding rate of electron transfer in the valence band can be expressed as

$$\frac{J_V}{J_{V,0}} = \left\{\frac{p_s}{p_{s,0}} \cdot \frac{[C_{red}]}{[C_{red,0}]} - \frac{[C_{ox}]}{[C_{ox,0}]}\right\} \tag{3.4.35}$$

$J_{V,0}$ is the exchange current density in the valence band at equilibrium. $p_{s,0}$ denotes the equilibrium surface concentration of holes. p_s represents the dynamic surface concentration of holes related to bulk surface hole concentration p_0 by:

$$p_s = p_0 \cdot e^{\frac{e\phi_{SC}}{kT}} \tag{3.4.36}$$

Under non-equilibrium conditions, the current-voltage relation can be described as

$$J_V = J_{V,0}\left[e^{\frac{e(V_E - V_0)}{kT}} - 1 \right] \tag{3.4.37}$$

Using equations (3.4.31), (3.4.33) (3.4.35) and (3.4.36), a relationship between the current densities in the valence and conduction bands is described:

$$\ln\left(\frac{J_{C,0}}{J_{V,0}}\right) = \ln\left(\frac{N_{CB}^*}{N_{VB}^*}\right) - \left(\frac{E_{BG} + 2\lambda}{2\lambda kT}\right)\cdot\left(\frac{E_{CB} + E_{VB}}{2} - E_{F,redox}\right) \tag{3.4.38}$$

N_{CB}^* and N_{VB}^* are the effective charge carrier densities at the conduction and valence band edges, λ the reorganization energy, and $E_{F,\ redox}$ the Fermi level of the redox system. By this model electron transfer occurs at the conduction band edge energy without loss. The rate constant is determined by the relative position of the energy states across the semiconductor-electrolyte interface, a topic extensively reviewed [11,55,58,64,65,87-96]. Various approaches to describe electron transfer reactions at semiconductor/liquid interfaces have been detailed, including the Lewis "electron-ball" model [89,90], Gerischer "half-sphere" model [91], tight binding approach [92], and adiabatic and non-adiabatic [91,93-95] transfer reactions.

Surface states can form due to abrupt distortion of the semiconductor crystal lattice. Charge transfer processes between surface states and the electrolyte have been analyzed in relation to water photoelectrolysis application [96]. Electron transfer mediated through surface states for an n-type semiconductor under dynamic equilibrium is shown in **Fig. 3.13(d)**.

Light Activity at the Interface

Light absorption by a semiconductor results in the creation of electron-hole pairs, by means of either direct or indirect momentum transitions depending on the crystal structure. Momentum is conserved in direct transitions, while a change in momentum is

required for indirect transitions. The light absorption coefficient (α) of such transitions is described by [97,98]:

Direct transition: $$\alpha = A' \sqrt{h\nu - E_{BG}} \tag{3.4.39}$$

Indirect transition: $$\alpha = A' \left(h\nu - E_{BG}\right)^2 \tag{3.4.40}$$

where A′ is a constant of proportionality. With light absorption by a semiconductor surface the free energy of both the minority and majority charge carriers shift leading to a non-equilibrium condition, quantified by quasi-Fermi energy levels E_F^*, that results in photocurrent and photovoltage generation at a semiconductor-electrolyte interface [11,55,65,75-77]. **Figure 3.14(a)** shows an n-type semiconductor in contact with an electrolyte showing photogeneration in the depletion region. The photocurrent of an n-type semiconductor absorbing monochromatic light with an absorption coefficient (α) is given by:

$$I_{ph} = eI_0 \left[1 - \left(1 + \alpha L_P\right) \cdot e^{-\alpha w}\right] \tag{3.4.41}$$

Where

$$L_P = \left(D_P \tau_p\right)^{1/2} = \left(kT \cdot \mu_p \tau_p\right)^{1/2} \tag{3.4.42}$$

The space charge region is denoted by length w, while L_P is the hole (minority carrier) diffusion length. τ_p is the minority carrier (hole) lifetime, μ_p the (minority carrier) hole mobility, and D_p the minority carrier diffusion coefficient.

$$w = L_D \left[\frac{\left(V - V_{FB}\right)}{kT}\right]^{1/2} \tag{3.4.43}$$

$$L_D = \left(\frac{2\varepsilon\varepsilon_0 kT}{eN_D}\right)^{1/2} \tag{3.4.44}$$

L_D is the Debye length of the space charge layer; a depth or distance greater than this leads to electron-hole pair recombination. Thus the magnitude of the quantum yield depends on the light penetration length $1/\alpha$ and the Debye length L_D [87,99]. At the flat band potential a finite current flows due to diffusion of minority carriers despite non-inclusion of surface recombination in this model. Schottky barriers play an important role in preventing electron-hole recombination by removing the majority charge carriers from the interface. For current transfer across the semiconductor-electrolyte interface a positive bias is needed for an n-type semiconductor, and negative bias for a p-type semiconductor. At equilibrium the initial amount of band bending between the bulk and surface in the space charge layer is given by:

$$\phi_{SC,0} = E_{F,redox} - V_{FB} \tag{3.4.45}$$

Using equation (3.4.13), equation (3.4.45) can be modified as

In the dark: $$\phi_{SC,0} = V_{redox} - V_{FB} \tag{3.4.46}$$

Under illumination, I: $$\phi_{SC,I} = V_{redox} - V_{FB} \tag{3.4.47}$$

Due to relatively slow rates of electron transfer between the semiconductor and the redox system, and/or trapping of minority carriers at surface states an additional driving force relative to the flat band potential is needed for the efficient photocurrent generation. A photovoltage arises with light illumination due to generation of electron-hole pairs that in turn decreases the band bending; ideal conditions for photocurrent generation from an n-type semiconductor, in the dark and under illumination, are shown in **Figs. 3.14(b)** and **3.14(c)** respectively. Correlating these two figures in the dark (equilibrium state) and under illumination (non-equlibrium) respectively with equations (3.4.46) and (3.4.47), the Gerischer model describes a threshold in illumination intensity as the driving force for water photoelectrolysis.

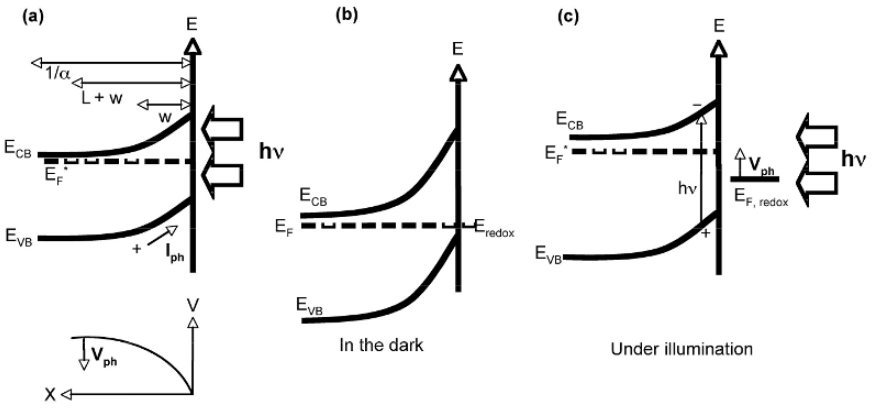

Fig. 3.14: (a) Photocurrent generation by electron-hole separation in an n-type semiconductor. Photovoltage arises through a decrease in the band bending across the depletion layer under light illumination. Energy bands of an n-type semiconductor-electrolyte interface: **(b)** in the dark, and **(c)** in the presence of light, with photogenerated free energy at open circuit represented by $eV_{ph} = E_{F,n}^{*} - E_{F,redox}$.

Under open circuit conditions the photovoltage of the interface can be expressed as:

$$V_{ph} = \frac{kT}{e} \cdot \ln \frac{I_{ph}}{I_0} = \frac{kT}{e} \cdot \frac{n_s^*}{n_{s,0}} \tag{3.4.48}$$

where I_{ph} is the minority carrier current and I_0 is the photon flux. Equation (3.4.48) shows a logarithmic dependence of the photogenerated free energy on the illumination intensity under equilibrium conditions.

Salvador [100] introduced a non-equilibrium thermodynamic approach taking entropy into account, which is not present in the conventional Gerischer model, formulating a dependence between the charge transfer mechanism at a semiconductor-electrolyte interface under illumination and the physical properties thermodynamically defining the irreversible photoelectrochemical system properties. The force of the resulting photoelectrochemical reactions are described in terms of photocurrent intensity, photoelectochemical activity, and interfacial charge transfer

mechanisms. The following relationships are given for a photoelectrochemical reaction based on hole transfer

$$h^+ + A^- \xrightarrow{K_P} A \tag{3.4.49}$$

where K_P is the rate constant for forward hole transfer reaction. With I_{ph} and V_{ph} representing the photocurrent and open-circuit photovoltage we have:

$$I_{ph} = e \cdot K_P \cdot p_{s,0}[A^-]\left\{e^{\frac{a_{ph}}{kT}} - 1\right\} \tag{3.4.50}$$

$$V_{ph} = \frac{1}{a_{ph}} \cdot \frac{kT}{e} \cdot \ln\left\{\frac{n_{s,0} \cdot K_{ET}[A]}{p_{s,0} \cdot K_P[A^-]}\right\} \tag{3.4.51}$$

$$\sigma = \frac{1}{w} \cdot \frac{I_{ph}}{e} \cdot \frac{a_{ph}}{T} \tag{3.4.52}$$

where

$$a_{ph} = kT \cdot \ln \frac{p_s^*}{p_{s,0}} \tag{3.4.53}$$

a_{ph} is the thermodynamic driving force of the photoelectrochemical reaction; K_{ET} is the rate constant for forward electron transfer reaction; σ is the entropy production with respect to stationary photocurrent (I_{ph}) under illumination; $n_{s,0} \approx n_s^*$, $p_{s,0} \approx p_s^*$ and $a_{ph} \geq E_{CB} - E_{redox}$. p_s^* (or n_s^*) are the surface excess population of holes under illumination (or electrons under illumination for electron transfer reactions).

3.5 Photoelectrochemical Cell Band Model

A common photoelectrolysis cell structure is that of a semiconductor photoanode and metal cathode, the band diagrams of which are illustrated in **Fig. 3.15** together with that of electrolyte redox couples. In **Fig. 3.15(a)** there is no contact between the semiconductor anode and metal cathode (no equilibrium effects communicated through the electrolyte). As seen in **Fig. 3.15(b)**, contact between the two electrodes (no illumination) results in

charge transfer from the semiconductor anode having a lower work function to the metal cathode having a higher work function until the work functions of both electrodes equilibrate. The result of this charge transfer is band bending by energy E_B. The energy levels of **Fig. 3.15(b)** are not favorable for water decomposition since the H^+/H_2 energy level is located above the cathode Fermi level. Under illumination, **Fig. 3.15(c)**, the photoanode surface potential and the (H^+/H_2) water reduction potential are each lowered, but the (H^+/H_2) water reduction potential still remains above the cathode Fermi level. Anodic bias is thus needed to elevate the Fermi level of cathode above the water reduction potential, see **Fig. 3.15(d)**, making the water splitting process feasible. This applied bias provides overvoltage at the metal cathode necessary to sustain the current flow, and increases the semiconductor band bending to maintain the required electric field driven charge separation in the semiconductor.

As illustrated by the example of **Fig. 3.15** external bias is an exceedingly useful tool for enabling operation of the photoelectrolysis cell to produce H_2 and O_2. The bias can be provided either by an external voltage (power) source, or by immersing the anode in a basic solution and the cathode in acidic solution. As illustrated by **Fig. 3.16**, several oxide semiconductors have flat band potentials above the H^+/H_2 level therefore no external bias is needed to produce H_2 and O_2. Unfortunately these oxide semiconductors have relatively large bandgap energies that result in low optical absorption, and hence low visible spectrum photoconversion efficiencies. In the first report on water photoelectrolysis by Fujishima and Honda [26], using an n-type TiO_2 anode and Pt cathode, it was observed that the photovoltage generated in the cell was not sufficient to carry out the water photolysis. An additional bias voltage of 0.25-0.50 V was required to achieve simultaneous oxygen evolution at the TiO_2 electrode and hydrogen evolution at the Pt cathode.

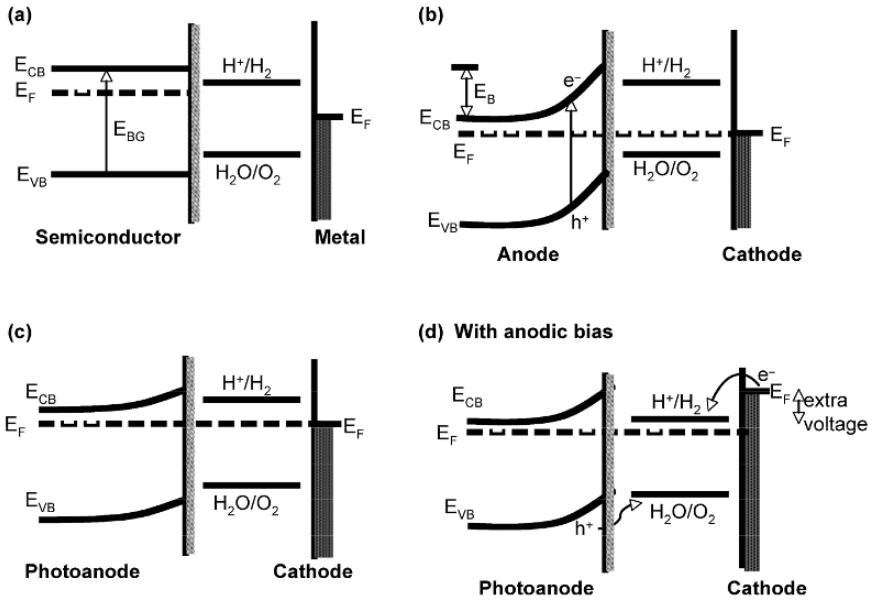

Fig. 3.15: Energy diagram of semiconductor-metal photoelectrolysis cell. **(a)** No contact and no chemical potential equilibrium; **(b)** galvanic contact in dark; **(c)** effect of light illumination; **(d)** effect of light illumination with bias. **(e)** Light illumination without bias, however in this case the semiconductor band edges straddle the redox potential for water photoelectrolysis.

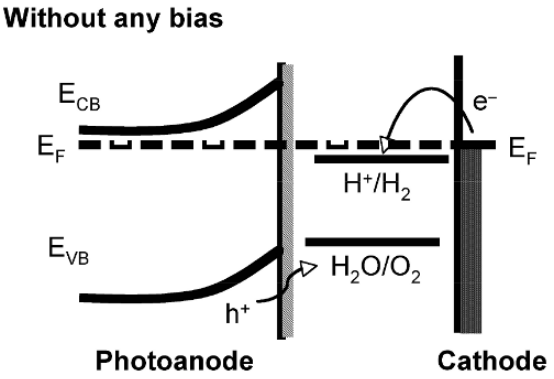

Fig. 3.16: Energy diagram of semiconductor-metal photoelectrolysis cell with light illumination without bias, however in this case the semiconductor band edges straddle the redox potential for water photoelectrolysis.

Another photoelectrolysis cell structure of considerable interest is that with both electrodes comprised of semiconductors, one n-type and the other p-type [31-35]. If the electron affinity of the n-type electrode is greater than that of the p-type electrode, when both electrodes are simultaneously illuminated the available electron-hole potential for driving chemical reactions is enhanced. Thus two photons, one at each electrode, are absorbed for the generation of one (minority carrier) electron-hole pair, a hole in the n-type semiconductor and an electron in the p-type semiconductor. Although the majority carriers recombine at the ohmic contacts a greater amount of potential energy is available to drive the chemical reactions. The energy diagram of such a system is shown in **Fig. 3.17**. The advantage in two semiconductor electrodes is that one can use a semiconductor of relatively smaller band gaps, able to capture a larger amount of solar spectrum energy, since the Fermi level of the majority carrier in the illuminated semiconductor does not have to be of energy suitable for driving the counter electrode reaction. In contrast to a single semiconductor electrode cell, a p-n photoelectrolysis cell does not require external bias when the flatband potential is below the H^+/H_2 level. Several p-n photoelectrolysis cells are reported using various semiconductor combinations such as TiO_2/p-GaP, n-TiO_2/p-CdTe, n-$SrTiO_3$/p-CdTe, n-$SrTiO_3$/p-GaP and n-Fe_2O_3/p-Fe_2O_3 [31-34].

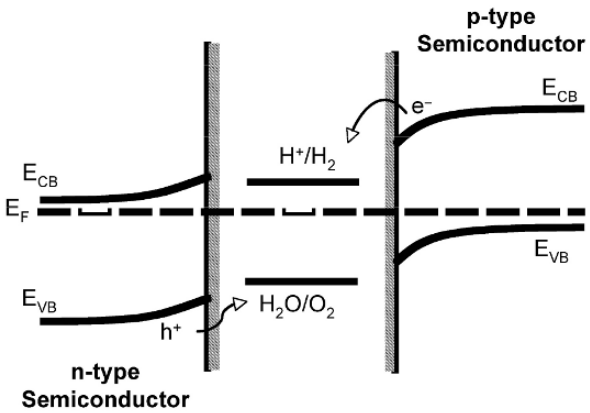

Fig. 3.17: Energy diagram for p-n photoelectrolysis cell.

The desire to eliminate the need for bias in a photoelectrolysis cell leads to another configuration where the anode and cathode are combined into a monolithic structure called a 'photochemical diode' [35]. A photochemical diode generally consists of a sandwich-like structure of an n-type/p-type bilayer connected through ohmic contacts. **Figure 3.18** shows the energy diagram for photochemical diodes consisting of a p-type/n-type bilayer electrode. This system resembles power generation in photosynthesis where two photoredox reactions are series coupled to drive water oxidation and CO_2 reduction. Both systems, photosynthesis and the photochemical diodes, require absorption of two photons to produce one useful electron-hole pair [11]. The n- and p-type semiconductors are analogous to photosystem II and photosystem I, and the majority carrier recombination at the ohmic contacts analogous to the recombination of photogenerated electrons from excited pigment II with the photogenerated holes in photosystem I. Unfortunately to date such devices generally face serious photocorrosion stability problems since both semiconductors must be stable in the same aqueous electrolyte solution, in the dark and under illumination.

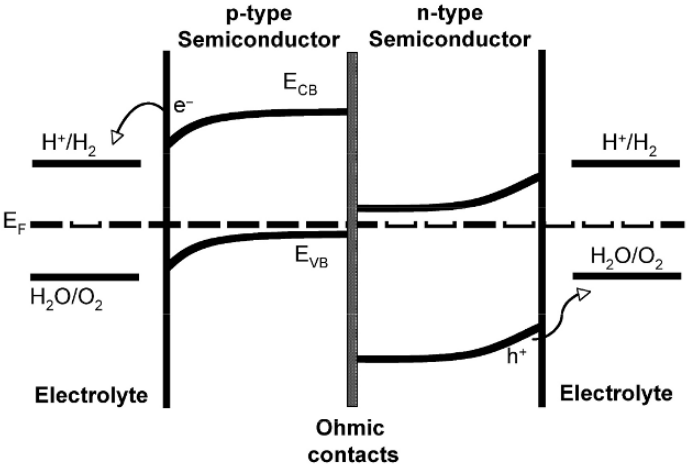

Fig. 3.18: Energy diagram for p-n photochemical diode for water photoelectrolysis.

3.6 Efficiency of Water Splitting in a Photoelectrochemical Cell

The usefulness of a water photoelectrolysis cell is primarily determined by the efficiency with which it converts light energy into chemical energy, which is stored in the form of hydrogen. In the case of water splitting, the redox properties of the electrolyte are fixed and hence the light harvesting and utilization properties of the light absorber, photoelectrode(s) or dispersed particles, decide cell efficiency. Since electric charges play an intermediate role in these cells, a knowledge about efficiencies related to production of electric charges by photons, charge injection into the external circuit and production of chemical energy by electric charges are useful for independently evaluating the corresponding functions of the absorber.

The light-to-electrical energy conversion efficiency measurements have their basis in photovoltaics and there are standard ways to determine these efficiencies. However, a sense of confusion prevails in the calculation of the light-to-chemical energy conversion, i.e. the overall photo conversion efficiency, due to the different definitions and cell configurations used by various research groups. Despite some isolated efforts seen in the literature to give a clear definition and methodology this is particularly significant in the case where an electrical bias is used to assist the water splitting. Different definitions given to efficiency and the correct methodology are discussed in this section.

The overall photoconversion efficiency is defined as the ratio of the maximum energy output that can be obtained from the final products, hydrogen and oxygen, to the energy supplied in the form of light to produce them. In terms of power, it can be defined as the ratio of the power density that can be obtained from hydrogen to the power density of the incident light. Since any practical photoelectrolysis system should operate using solar energy, before going to the various formula and methodologies used to calculate the efficiency, it is worth looking at limitations on the solar energy to hydrogen energy conversion efficiency in an ideal case.

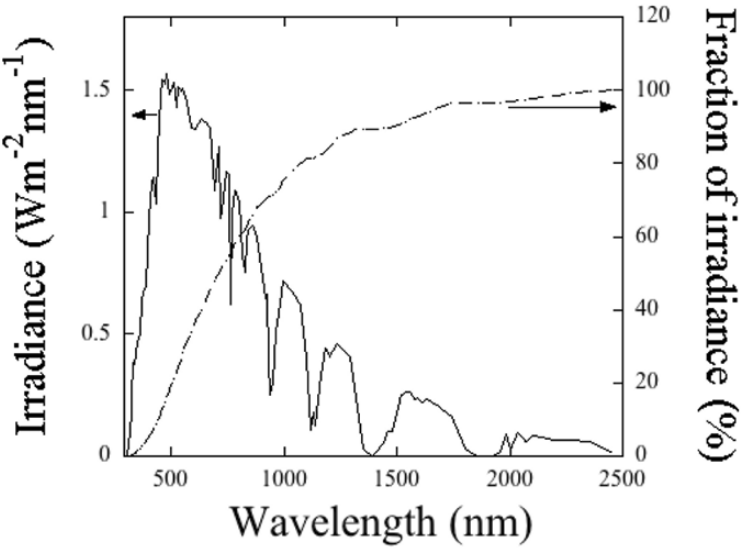

Fig. 3.19a: Solar spectral irradiance (global AM1.5) and the fraction of the irradiance above λ_{min} where λ_{min} is the minimum wavelength at which the spectral irradiance has a measurable value [101].

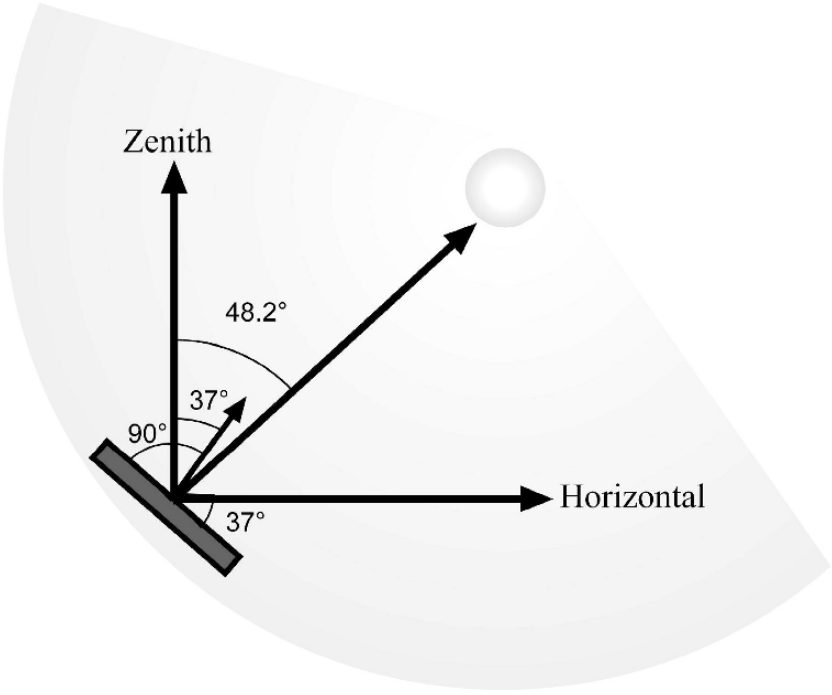

Fig. 3.19b: Configuration for AM1.5 solar illumination.

The solar energy available for conversion depends upon the relative position of the sun to the absorbing plane, and atmospheric conditions. **Figure 3.19a** shows a representative solar spectral irradiance under the global AM 1.5 (air mass 1.5) condition [101]. AM 1.5 represents the average atmospheric conditions in the United States. AM 1.5 corresponds to a situation when the absorber plane is inclined 37° towards the equator and sun is at a zenith angle of 48.19° (AM=1/COS48.19=1.5)as shown in **Fig. 3.19b**. 37° is the average latitude for the 48 contiguous states of the U.S.A. In such a configuration, the light travels through the atmosphere 1.5 times the distance it travels when the sun is at 0° zenith angle (AM 1.0). The global irradiance includes both direct and diffused components of light from the sun. The total irradiance can be calculated as:

$$P_t = \int_0^\infty P(\lambda)\, d\lambda \tag{3.6.1}$$

The total irradiance is about 964.1 W/m^2. However, considering the effect of variations in the atmospheric conditions (such as cloudiness, dust particles and relative humidity), the spectrum is normalized to 1000 W/m^2. This is generally regarded as 1 sun. Photoelectrochemical water splitting is represented by the reaction:

$$H_2O_{(liquid)} + 2h\nu \rightarrow \tfrac{1}{2}\, O_{2(gas)} + H_{2(gas)} \tag{3.6.2}$$

As discussed in Chapter 2, a minimum energy of 1.229eV per electron should be supplied to split water. A minimum of two quanta (photons) are needed to generate one molecule of hydrogen. 1.229eV corresponds to 1010 nm and hence about 77% of the solar energy is available for water splitting (see the fraction of irradiance above λ_{min} given in **Fig. 3.19a**).

The basic parameter deciding the light harvesting ability of the photoelectrode is the bandgap E_g of the material. There are inherent losses associated with any solar energy conversion processes involving materials [102-105]. These losses include: {1} Only the energy $E \geq E_g$ (or the photons with wavelength $\lambda \leq \lambda_g$ where λ_g is the wavelength corresponding to the bandgap) is absorbed and the rest is lost [102,105]. {2} Of the absorbed

energy, the excess energy which is the difference in the energy of the absorbed photon and the band gap energy (E - E_g) is lost as heat during the relaxation of the absorber to the level of E_g. {3} The energy of the excited state is thermodynamically an internal energy that has the entropy term involved in it and only a fraction (up to about 75%) of this energy can be converted into work (electrical energy) or stored as chemical energy. {4} Although commonly negligible, losses due to spontaneous emissions such as fluorescence also contributes to the efficiency limitations.

The limiting efficiency ε_{limit} of a solar energy conversion process is [102,103]:

$$\varepsilon_{\lim it} = \frac{F_g \, \Delta\mu_x \, \phi}{P_t} \tag{3.6.3}$$

where F_g is the absorbed photon flux given by

$$F_g = \int_{\lambda_{\min}}^{\lambda_g} \frac{P(\lambda)}{(hc/\lambda)} d\lambda \tag{3.6.4}$$

$\Delta\mu_x$ is the chemical potential of the excited state relative to the ground state and ϕ is the internal quantum efficiency which is the fraction of the excited states utilized for the generation of a useful product. The chemical potential is related Gibbs energy by $G = \Sigma_i^n \, \mu_i \, N_i$ where μ_i is the chemical potential of the i^{th} state and N_i is the number of i^{th} states, which is the maximum energy available to do work or to be stored as chemical energy. The ideal limiting efficiency in the case of single bandgap devices (devices involving single photosystem) is shown in **Fig. 3.20** [102,103]. A maximum of 33% is possible at about 900 nm for single bandgap devices. This value is higher for dual photosystems. The maximum value of solar irradiance efficiency ε_g corresponds to semiconductors of $1.0 \leq E_g \leq 1.4$ ev [106,107]. Hanna and Nozik [108] have recently calculated the limiting efficiency of a two band gap tandem device without carrier multiplication (i.e., when more than one electron-hole pair are generated by a single photon) as 40% and with carrier multiplication as 46%.

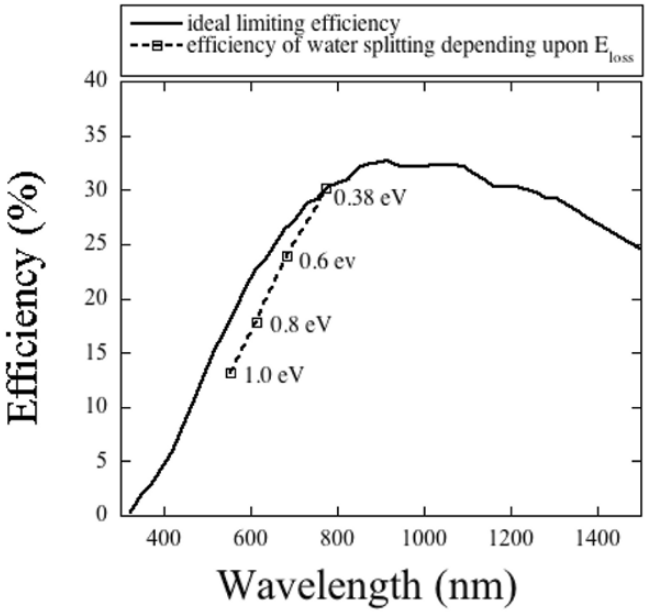

Fig. 3.20: The ideal limiting solar conversion efficiency for single bandgap devices. The dotted line shows efficiency of photoelectrolysis cells at different values of E_{loss} in relation (3.6.8) [102].

In the case of photoelectrolysis cells involving semiconductors, the three major processes leading to water splitting are the absorption of photons of energy $E \geq E_g$, conversion of absorbed photons into electric charges (or excited states) and utilization of electrical charges (conversion of excited states) for water splitting. The overall solar energy conversion efficiency ε_o can be written as the product of the efficiencies of the cell in performing these processes:

$$\varepsilon_o = \varepsilon_g \, \phi \, \varepsilon_c \tag{3.6.5}$$

ε_g is solar irradiance efficiency, ϕ is the quantum efficiency and ε_c the chemical efficiency. ε_g is defined as the fraction of the incident solar irradiance with photon energy $E \geq E_g$, given by:

$$\varepsilon_g = \frac{F_g E_g}{P_t} = E_g \frac{\int_{\lambda_{\min}}^{\lambda_g} \frac{P(\lambda)}{(hc/\lambda)} d\lambda}{\int_0^{\infty} P(\lambda)\, d\lambda} \quad OR \quad \varepsilon_g = E_g \frac{\int_{E_g}^{\infty} N(E)\, dE}{\int_0^{\infty} E\, N(E)\, dE} \qquad (3.6.6)$$

N(E) is the distribution of photons with respect to their energy. ϕ is given by

$$\phi = \frac{N_E}{N_T} \qquad (3.6.7)$$

N_E is the number of photons utilized for electron-hole pair generation and N_T is the total number of absorbed photons. ϕ =1 in the ideal case where all the photons of energy $E \geq E_g$ are utilized for carrier generation.

The chemical efficiency, ε_c, is the fraction of excited state energy converted to stored chemical energy and given by:

$$\varepsilon_c = \frac{E_g - E_{loss}}{E_g} \qquad (3.6.8)$$

E_{loss} is the actual energy loss per molecule involved in the overall light energy to chemical energy conversion process. E_{loss} always has a value greater than zero due to the entropy change (the term $T\Delta S$) involved in the process. In the ideal case (ϕ=1) it has a value E_g - (ΔG^0/n) where n is the number of photons required to drive reaction (1) and ΔG^0 is the standard Gibbs energy of the reaction. Considering (3.6.6)-(3.6.8), the ideal ε_o (ϕ=1) can be written as [109]

$$\varepsilon_o = \frac{F_g \Delta G (1 - \phi_{loss})}{P_t} \text{ if } E_g \geq \Delta G^0 + E_{loss} \qquad (3.6.9)$$

where ϕ_{loss} is the radiative quantum yield which is the ratio of re-radiated photons to absorbed photons. ε_o is 0 for $E_g < \Delta G^0 + E_{loss}$ in

the ideal case. The ϕ_{loss} corresponding to the maximum value of efficiency is given by $\phi_{loss} \approx [\ln (F_g/F_{bb})]^{-1}$ where F_{bb} is the blackbody photon flux at wavelengths below the bandgap wavelength.

Although the minimum bandgap needed for water splitting is 1.23 eV, the entropy consideration in E_{loss} necessitates materials with significantly higher bandgaps. The maximum photoconversion efficiencies corresponding to different values of E_{loss} for single bandgap devices are shown in **Fig. 3.20** [102,103]. For a device involving single photosystem (single bandgap) where minimum two photons are required for the reaction (3.6.1), the ideal limit of ε_o is 30.7% corresponding to a wavelength of 775 nm (1.6eV) and E_{loss} 0.38 eV (**Fig. 3.20**). That is, a minimum bandgap of 1.6 eV is required for the photelectrode used for water splitting using solar radiation. In the case of dual photosystems involving two bandgaps and absorption of four photons, the ideal limit is 41%. In practical systems E_{loss} takes values greater than 0.8 eV due to other loss factors. These losses include those due to transport of electrons within the electrode during charge separation, transport of electrons from photo-electrode to counter electrode (for n-type materials this is from photoanode to cathode), transport of electrons/holes to the photoelectrode/electrolyte interface, Joule heating due to the electron flow through external circuit and the cathodic and anodic overpotentials. The overvoltages associated with electrodes are functions of mechanisms of the electrode reactions, current density, structures of the electrodes, surface properties of the electrodes, temperature, composition of electrolyte and similar factors [106]. Considering all these losses, E_{loss} has a value [110]:

$$E_{loss} \geq 0.5 + e\,(\eta_a + \eta_c + IR)\ eV$$

Where η_a and η_c are, respectively, the anodic and cathodic overpotentials. Considering all these losses an optimum bandgap of 2.0 to 2.25 eV is required for the materials used as photoelectrodes for water photoelectrolysis. In practical cases, a reasonable value of overall solar efficiency is 10% for single bandgap devices involving two photons and 16% for dual photosystem devices involving 4 photons [102,103,110,111].

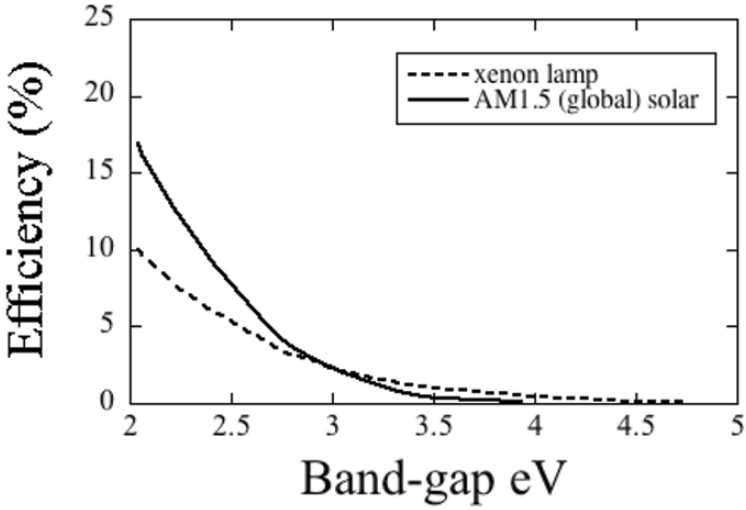

Fig. 3.21: Maximum efficiency possible depending upon semiconductor bandgap, under xenon arc lamp and AM1.5 solar illuminations.

In research laboratories, different types of light sources are used instead of solar radiation. In most cases the simulated spectrums have considerable deviation from the solar spectrum. Based on equation (3.6.9) Murphy et al [109] analyzed the maximum possible efficiencies for different materials according to their band gap in the case of solar global AM 1.5 illumination and xenon arc lamp, see **Fig. 3.21**. For example, anatase titania with a bandgap of 3.2 eV has a maximum possible efficiency of 1.3% under AM 1.5 illumination, and 1.7% using Xe lamp without any filter. For rutile titania these values are 2.2% and 2.3% respectively.

In practical cases the absorption edge is not sharp and absorption coefficients of semiconductors decrease as the wavelength approaches the bandgap wavelength. The absorbed photon flux can then be written as [109]

$$F_x = \int_0^{\lambda_g} \alpha(\lambda) P(\lambda) d\lambda \text{ where } \alpha(\lambda) = 1 - e^{-k(\lambda)h} \qquad (3.6.10)$$

k is the absorption coefficient and h is the thickness of the semiconductor. Hence for lower thickness electrodes where path

length is not enough for complete light absorption the efficiency decreases. Reflections from the sample and electrolyte containers, as well as absorption in electrolyte also reduce the efficiency of the cell [109].

The difference between photoelectrochemical solar cells and photoelectrochemical water splitting is that in the former case free energy (electrical energy) is produced but the net gain is zero whereas in photoelectrochemical water splitting there is a net gain in free energy (from hydrogen). In both cases, free energy appears as the photo voltage between the electrodes that drives the electric charges through the circuit or supplies carriers for hydrogen/oxygen generation during illumination; at zero current this is termed the open circuit voltage. When short-circuited, the photovoltage goes to zero and current becomes maximum. Under dark conditions, the Fermi levels of the semiconductor photoelectrode and counter electrode, redox potential of the electrolyte equalize when short circuited and the valence band and conduction band are bent up to $E_f - E_{redox}$ where E_f is the Fermi level of the semiconductor and E_{redox} is the potential of the redox couples in the solution [112]. The barrier height represents the upper limit of the open circuit voltage that can be achieved under high irradiance. Upon irradiation, say in the case of n-type semiconductors, the conduction band population of electrons increases and the Fermi level shifts up and conduction band bending reduces. Now the difference between the electrochemical potential of electrons in the semiconductor (Fermi level) and the chemical potential of electrons in the solution (the redox potential) gives the open circuit voltage. V_{oc} cannot exceed $|E_f - E_{vb}|$ for photoanodes where E_{vb} is the valence band energy. Therefore, the open circuit potential can never be as high as the bandgap potential [102,112]. As mentioned earlier in the discussion on the fundamental limitations on attainable efficiency, this is a consequence of the fact that the energy of the excited state is thermodynamically an internal energy and not Gibbs energy due to the entropy term ($\Delta G=U+PV-T\Delta S$). Up to about 75% of the internal energy can be converted into free energy [102]. Hence, higher band gap materials are useful for water splitting as these can supply higher V_{oc} even exceeding 1.229 eV and hence the possibility of water splitting without supplying any additional electrical energy.

However the higher band gap materials cannot effectively utilize solar energy. Therein of course lies the difficulty. In practical cases, V_{oc} values up to about 1 V are common.

Though equation (3.6.5) is more useful for analyzing the performance of photoelectrolysis cells, for practical purposes the photoconversion efficiency (solar conversion efficiency if sunlight is used) is calculated by modifying (3.6.5) in the form

$$\varepsilon_o = \frac{\Delta G^0 R_{H_2}}{P_t} \tag{3.6.11}$$

R_{H2} is the rate of production (moles/s) of hydrogen in its standard state per unit area of the photoelectrode. The standard Gibbs energy ΔG^0 = 237.2 kJ/mol at 25°C and 1 bar, and P_t is the power density (W/m^2) of illumination. The numerator and denominator have units of power and hence, as in the case of photoelectrochemical solar cells, the photoconversion efficiency is the ratio of power output to the power input.

Equation (3.6.11) is based on the assumption that the free energy ΔG^0 can be completely retrieved in an ideal fuel cell run by the products from the photoelectrolysis cell for which the relation is applied. Instead of the free energy ΔG^0, the enthalpy (heat) of water splitting ΔH^0 also has been used in some cases. Here, it is assumed that the heat of water splitting is completely retrieved by burning hydrogen. At 25°C and 1 bar, ΔH^0= 285kJ/mol. However, due to the similarity in functioning of photoelectrolysis cells and photoelectrochemical solar cells where the free energy term V_{oc} is used to calculate the efficiency, ΔG^0 is commonly used in (3.6.11).

If I is the current density responsible for the generation of hydrogen at the rate of R_{H2} in (3.6.11), then under 100% Faradaic conversion (that is, all the carriers are utilized only for generating hydrogen/oxygen), R_{H2} = I/nF. The voltage corresponding to the Gibbs energy is $V_{rev} = \Delta G^0/n\,F$ = 1.229 V as n, the number of moles of electrons used for generating one mole of hydrogen, is 2.

$$\varepsilon_o = \frac{1.229\ I}{P_t} \tag{3.6.12}$$

When ΔH^0 is used in (3.6.11), 1.229 V in (3.6.12) needs to be replaced by 1.482 V.

Spontaneous water-splitting upon illumination needs semiconductors with appropriate electron affinity and flat band conditions. The flat band positions shift with electrolyte pH. Hence, an external bias needs to be applied between the electrodes in most cases to effect water splitting. The external bias can be either electrical or chemical. This external bias contribution should be subtracted from (3.6.11) or (3.6.12) to get the overall photoconversion efficiency. In the case of an external electrical bias, the efficiency can be defined as:

$$Efficiency\ \varepsilon_0 = \frac{energy\ \ stored\ as\ hydrogen - Energy\ input\ \ from\ \ power\ \ supply}{Light\ energy\ input}$$

$$\varepsilon_o = \frac{\Delta G^0\, R_{H_2} - V_{bias}\, I}{P_t} \qquad (3.6.13a)$$

OR

$$\varepsilon_o = \frac{(1.229 - V_{bias})\ I}{P_t} \qquad (3.6.13b)$$

The basis of this definition is that a fuel cell run by the products from the photoelectrolysis cell supplies a part of its output to the photoelectrolysis cell as electrical bias. The combined system must have a significant positive energy output to be considered as useful.

Practical photoelectrolysis cells consist of two electrodes immersed in the electrolyte and the bias voltage is applied between the working and counter electrodes [113]; the overall chemical reaction in such a cell is made of two independent half-reactions. In laboratory water photoelectrolysis experiments, to understand the chemical changes at the photoelectrode a three-electrode geometry is used to measure photocurrent. This geometry involves a working electrode (photocathode or photoanode), a counter electrode which generally is platinum, and a reference electrode. The internationally accepted primary reference is the standard hydrogen electrode (SHE) or normal hydrogen electrode (NHE) which has all

components at unit activity [(Pt/H_2 (a=1)/H^+ (a=1, aqueous)]. However, using such an electrode is impractical and hence other reference electrodes such as silver-silver chloride (Ag/AgCl/KCl) and saturated calomel electrodes (SCE) ($Hg/Hg_2Cl_2/KCl$) are generally used. Their potentials may then be converted in terms of Normal Hydrogen Electrode potential (NHE). The potential of Ag/AgCl electrode is 0.197 V vs NHE and that of SCE is 0.242 V vs NHE [114].

Equation (3.6.13) gives a thermodynamical measure of the efficiency and is generally applied in a two-electrode configuration. Nevertheless, different approaches have been followed by various groups to find the efficiency, especially when a three- electrode geometry is used [115-117]. This makes a direct comparison of reported efficiency values meaningless. Some of these approaches are discussed below.

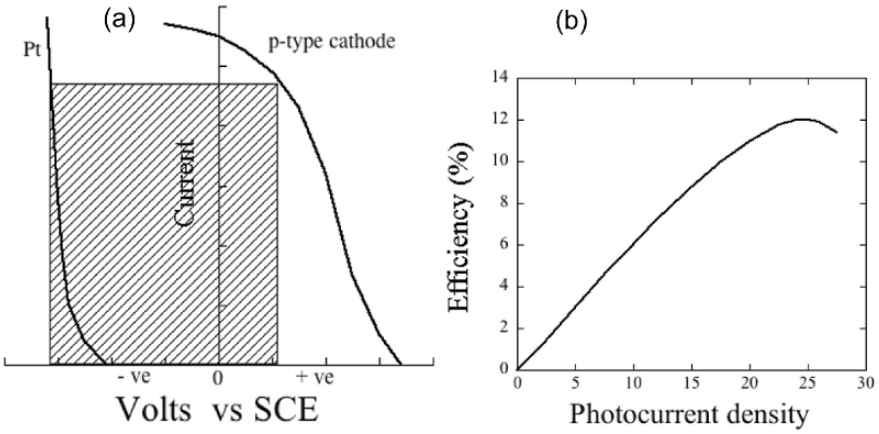

Fig. 3.22: (a) Current – voltage characteristics of a p-type photocathode and that when it is replaced by a platinum shown to illustrate the efficiency calculation using the power saving approach. The shaded area represents the maximum power saving as a result of photoelectrolysis. **(b)** The efficiency at various photocurrent densities obtained useing the base graph.

One approach to find efficiency uses the electrical power saved due to the use of light in a photoelectrolysis process compared to an electrolysis process using light-insensitive electrodes [118].

$$\varepsilon_o = \frac{P_{saved}}{P_t} = \frac{V_{save}\, I}{P_t} \tag{3.6.14}$$

The method involves recording the current from a semiconductor photoelectrode (anode or cathode) at various applied potentials and then repeating the experiment by replacing this semiconductor electrode with a metal electrode like platinum. For example **Fig. 3.22(a)** shows the current-voltage relationship of a hydrogen evolving p-type cathode in 1 M $HClO_4$, and the same relationship when the electrode is replaced by a platinum cathode [119,120]. The power saved P_{saved} for a particular current density I, is V_sI where V_s is the difference between the corresponding voltages for semiconductor and metal cathodes. A representative graph showing the relation between photocurrent density and efficiency [equation (3.6.14)] is given as **Fig. 3.22(b)**.

The power saving is maximum when both electrodes operate at a current density (I_{max}) and a voltage corresponding to the maximum power conversion point in the photoelectrolysis process. The maximum power saved as a result of photoelectrolysis is shown as the shaded area in **Fig. 3.22(a)**.

$$\varepsilon_{o\max} = \frac{\Delta V_{\max}\, I_{\max}}{P_t} \tag{3.6.15}$$

Here $\Delta V_{max} = V_{save(max)}$ represents the difference in voltages at the semiconductor electrode and metal electrode at the maximum power conversion point. For example, in their experiment using a p-type InP photocathode, Heller and Vadimsky [120] obtained a current 23.5 mA/cm^2 at maximum power point. A voltage of 0.11V vs SCE was applied in the case of InP electrode and -0.33V vs SCE in the case of platinum electrode, to obtain this current. Thus, the maximum saved voltage ΔV_{max}= 0.11-(-0.33) V= 0.43V. Therefore, P_{saved}=0.43 V x 23.5 mA/cm^2 = 10.1mW/cm^2. As they used a solar illumination of 84.7 mW/cm^2, the efficiency is 11.9%.

An issue in using this approach is that equations (3.6.14) and (3.6.15) involve overpotential losses. Hence highly catalytic metal electrodes with low overpotential are required for comparison. If a metal electrode with a low catalytic activity is used these equations yield exaggerated values for photoconversion efficiency.

An approach similar to this avoids the use of a comparative noble metal electrode and neglects overpotential losses at the electrodes. In this method, the potential applied at the hydrogen (or oxygen) electrode (in a three electrode configuration) is compared with the potential generated at an ideal fuel cell anode (or cathode). In the case of a n-type semiconductor photoanode:

$$\varepsilon_0 = \frac{\left(V_{ox}^0 - V_{app}\right) I}{P_t} \quad \text{(oxygen evolution using photoanodes)} \quad (3.6.15a)$$

or

$$\varepsilon_o = \frac{(V_{app} - V_{H_2}^0)\ I}{P_t} \text{ (hydrogen evolution using photocathodes)} \quad (3.6.15b)$$

V_{ox}^0 and $V_{H_2}^0$ represent the standard potentials of oxygen and hydrogen electrodes respectively. V_{ox}^0 takes a value of +0.401 V vs NHE in alkaline electrolytes (pH=14) and +1.229V vs NHE in acidic electrolytes (pH=0). The corresponding values of $V_{H_2}^0$ are -0.828 V vs NHE and 0 V vs NHE. For example, Ang and Sammells [116] reported on obtaining a photocurrent of 24 mA in a p-type InP cathode at –0.65V vs SCE (i.e. 0.408 V vs NHE) in KOH electrolyte. Thus the efficiency calculated using equation (3.6.15b) ($V_{H_2}^0$ = -0.828V vs NHE) is 10.1%.

Another form of this definition [equation (3.6.15)] has sparked much debate in the scientific community [121-124]. In this approach V_{app} (or V_{bias}) is taken as the absolute value of the difference between the potential at the working electrode measured with respect to a reference electrode (V_{meas}) and the open circuit potential (V_{oc}) measured with respect to the same reference electrode under identical conditions (in the same electrolyte solution and under the same illumination). In the case of a semiconductor photoanode where oxygen evolution takes place the efficiency is calculated as:

$$\varepsilon_0 = \frac{I_P \left(V_{rev}^0 - \left|V_{app}\right|\right)}{P_t}$$

$$\varepsilon_o = \frac{I\left(V_{rev}^0 - \left|V_{meas} - V_{aoc}\right|\right)}{P_t} \quad (3.6.16)$$

V^0_{rev} = 1.229V is the standard state reversible potential for the water splitting reaction and V_{aoc} is the anode potential at open circuit conditions. Term V_{meas}-V_{aoc} arises from the fact that V_{oc} represents the contribution of light towards the minimum voltage needed for water splitting potential (1.229V) and that the potential of the anode measured with respect to the reference electrode V_{meas} has contributions from the open circuit potential and the bias potential applied by the potentiostat (i.e. V_{meas}= V_{app}+V_{aoc}). The term V_{meas}-V_{aoc} makes relation (3.6.16) independent of the electrolyte pH and the type of reference electrode used. Thus the use of V^0_{rev} in relation (3.6.16) instead of V^0_{ox} or V^0_{H2} as in the case of relation (3.6.15) is justified.

Although this approach has received wide attention and is being commonly used, there is skepticism that the efficiency values obtained using relation (3.6.16) gives exaggerated photoconversion efficiency values. In either the two electrode or three electrode geometry the voltage measured between the working and the counter electrodes gives the actual bias voltage $V_{app(wc)}$ applied (voltage in excess of the open circuit voltage). However in practice, where a potentiostat is used to apply an external bias to the photoelectrode, this actual voltage ($V_{app(wc)}$) may exceed the bias voltage measured as V_{app}=V_{meas}-V_{aoc} with respect to the reference electrode [125]. Thus the use of the latter term in (3.6.16) can show a higher value for efficiency than when the term $V_{app(wc)}$ is directly used as in the case of relation (3.6.13).

Figure 3.23 is plotted to demonstrate the difference in the efficiency values calculated by different approaches represented by relations (3.6.13), (3.6.15a) and (3.6.16). A two electrode geometry was used for photocurrent measurements and efficiency calculation using relation (3.6.13) and a three electrode geometry was employed for relations (3.6.15a) and (3.6.16). A 6 μm long titania nanotube array film (polycrystalline) on titanium foil was used as the photoanode. Platinum served as the counter electrode and the 1M KOH solution as the electrolyte. In the three electrode configuration, an Ag/AgCl reference electrode was used to measure the photoanode potentials. As the titania bandgap is 3.0 to 3.2 eV (depending upon whether the crystalline phase is rutile or antase), a near UV light illumination (320-400nm) from a 50W metal-hydride lamp was

used. For the two electrode geometry a Keithley source meter (model 2400) and for the three electrode geometry a potentiostat (CH Instruments, model CHI 600B) was used to apply the bias. The x-axis of the plot (**Fig. 3.23**) shows the voltage measured between the working (titania nanotube array) and counter electrodes for relation (3.6.13) and the potential at the photoanode anode measured with respect to Ag/AgCl reference electrode for relations (3.6.15a) and (3.6.16).

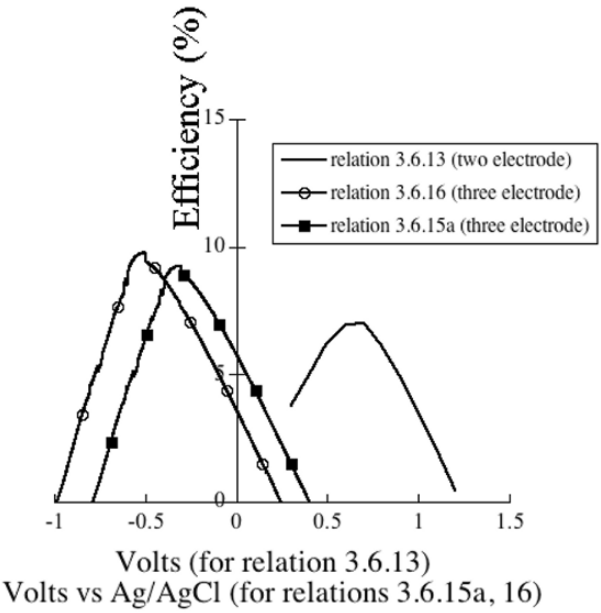

Fig. 3.23: Efficiency under near UV illumination of a photoelectrochemical cell comprised of a titania nanotube array photoanode and Pt counter electrode. For the calculation of efficiency using equation (3.6.13), a two electrode geometry was used while for the calculation using equations (3.6.15a) and (3.6.16), a three electrode geometry was used.

It can be seen from **Fig. 3.23** that the relation (3.6.16) yielded the highest efficiency of about 9.5% whereas the efficiency calculated using relation (3.6.13) employing a two-electrode geometry has a maximum value of about 7%. Although the relative values may vary with respect to the experimental setup and measurement conditions, this exercise demonstrates that a certain

degree of exaggeration could occur in the efficiency values calculated using (3.6.16) in a three electrode geometry. Also, note that the efficiency shown is not the solar photoconversion efficiency. The value of solar photoconversion efficiency is much lower (discussed later).

Figure 3.23 shows that the efficiency calculated using (3.6.13) in a two-electrode geometry is maximum at a bias voltage of about +0.65 V. As discussed above, in the case of a three electrode geometry, the bias is calculated as $V_{app} = V_{meas} - V_{aoc}$. With a V_{aoc} of about -0.98 V vs Ag/AgCl and V_{meas} of about –0.5 V vs Ag/AgCl corresponding to the point of maximum efficiency, V_{app} takes a value of about +0.48 V. Thus, the actual bias applied between the working and the counter electrodes is higher (by 0.17 V) compared to the bias measured with respect to the reference electrode.

Replacement of V^0_{rev} in relation (3.6.16) by a term $V^0_{rev} + V_{overvoltage}$ was also suggested [126]. That is, overvoltage losses are added to the work output from hydrogen. This gives unrealistic values for efficiency as the efficiency increases with increased overvoltage losses at the working and counter electrodes. Furthermore, even by burning hydrogen such an amount of energy cannot be retrieved. However in some cases it is considered that the hydrogen is burnt to retrieve the energy, and the thermoneutral potential 1.48 V is used in equation (3.6.13) instead of 1.229 V [127].

A criticism often seen in the literature regarding use of relation (3.6.13) and its different forms is that it gives negative efficiency values. It should be noted that negative efficiency signifies that the bias voltage exceeded 1.229 V and the regime has changed from photoelectrolysis to direct electrolysis. That is, the minimum energy needed for water splitting is completely provided by the external power supply [122]. In a carefully done work, Murphy et al. [109] measured photocurrent using a three electrode geometry but the efficiency was calculated using (3.6.13) with the V_{bias} taken as the voltage between working and counter electrodes. It appears that any meaningful efficiency calculation should use (3.6.13) in three or two electrode geometry with V_{bias} measured between counter electrode and working electrode [117,128-130].

In addition to (3.6.13), (3.6.15) and (3.6.16) other approaches exist to calculate the efficiency. However, these are not considered to effectively represent the actual ability of the cell to convert light energy into chemical energy. One such definition for efficiency [131] is

$$\varepsilon_o = \frac{V_{rev}^0 \, I}{\left(P_t + I V_{bias}\right)} \tag{3.6.17}$$

However this relation does not yield a solar conversion efficiency but gives the throughput efficiency for the device [115]. Furthermore, it is insensitive to the contribution from light and only approaches zero at a bias voltage much higher than 1.229 V that can be regained in an ideal fuel cell. For the case where the photoelectrolysis cell supplies the input for the fuel cell and a part of the electrical energy output from the fuel cell is used to bias the phototoelectrolysis cell, relation (3.6.17) is modified as [131]:

$$\varepsilon_o = \frac{(V_{rev}^0 - V_{bias}) I}{\left(P_t + I V_{bias}\right)} \tag{3.6.18}$$

Recently, Raja et al. [132] proposed a method to calculate efficiency. In this method, the power output by the three-electrode photoelectrochemical cell is calculated by considering the voltage increase between the anode and cathode due to light illumination under external bias conditions.

$$\varepsilon_o = \frac{I_p \, \Delta E}{P_t} \tag{3.6.19}$$

I_p is the photocurrent density in mA cm^{-2}, ΔE the potential difference between working electrode and counter electrode under illumination minus the potential difference between the same electrodes without illumination (dark). That is, ΔE is the photovoltage with dark voltage subtracted from it. This equation is misleading and has no thermodynamics basis. ΔE does not necessarily represent the sample behavior but it depends upon the experimental conditions. Furthermore the hydrogen produced at current I_p can yield a power output higher than $I_p \, \Delta E$.

When a chemical bias is used instead of electrical bias, Ghosh and Maruska [133] defined efficiency in terms of heat of combustion of 1 mole of hydrogen (285.6 kJ) and heat of neutralization of 2 moles of H^+ (117.6kJ) [134] as:

$$\varepsilon_o = \frac{\frac{I}{nF}(285600 - 117600)}{P_t} \tag{3.6.20}$$

where n = 2, F = 96485 Coulombs. In the case of two-photoelectrode geometry involving an illuminated p-type anode and an illuminated n-type cathode, where light energy is converted to both chemical and electrical energy, Kainthla et al. [135] used the formula

$$\varepsilon_o = \frac{1.23I + IV_{cell}}{2P_t} \tag{3.6.21}$$

The chemical energy output is given by $1.23I$ while the electrical energy output is given by IV_{cell}. The factor of 2 is included to take into account the simultaneous illumination of both electrodes of equal area.

A very useful parameter for evaluating the performance of a photoelectrolysis cell is the incident photon to current conversion efficiency (IPCE). This is a measure of the effectiveness in converting photons incident on the cell to photocurrent flowing between the working and counter electrodes. IPCE is also called the external quantum efficiency.

$$IPCE = \frac{I_p(\lambda)}{eF(\lambda)} \tag{3.6.22a}$$

or

$$IPCE = \left(\frac{hc}{e}\right)\left(\frac{I_P(\lambda)}{P(\lambda)\,\lambda}\right) \tag{3.6.22b}$$

or

$$IPCE = 1240\,\frac{I_p(\lambda)}{P(\lambda)\lambda} \tag{3.6.22c}$$

$I_p(\lambda)$ is the photocurrent density at wavelength λ. IPCE becomes 100% when all photons generate electron-hole pairs. However, in practical situations IPCE is always less than 100% due to the losses corresponding to the reflection of incident photons, their imperfect absorption by the semiconductor and recombination of charge carriers within the semiconductor, etc.

IPCE is calculated by measuring the current in a cell when a particular wavelength or a small group of wavelengths (band pass, usually up to 12 nm) with a known power density $P(\lambda)$ incident on it. It is usually measured at a bias voltage corresponding to the maximum power point (voltage corresponding to the peak efficiency in **Fig. 3.23**). The IPCE of a titania nanotube array biased at 0.5 V illuminated using wavelengths from a 300 W xenon arc lamp and monochromator (cornerstone 130) at a band pass of 4 nm is given in **Fig. 3.24**. The nanotube has a band gap of about 3.0 - 3.2 eV corresponding to antase-rutile mixed phase and hence the IPCE reduces to zero at the wavelength corresponding to the bandgap.

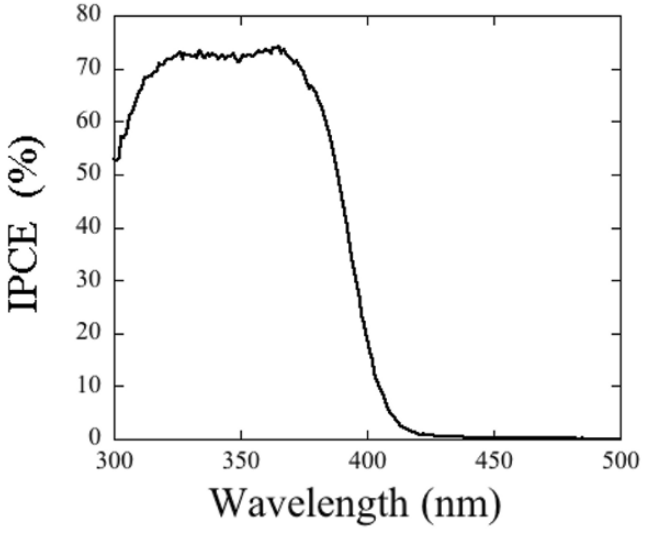

Fig. 3.24: Incident photon to current efficiency (IPCE) spectrum of a titania nanotube array photoelectrode.

IPCE enables the estimation of the total photocurrent as well as efficiency of a photoelectrolysis cell under any type of

illumination, say for example global sunlight [136]. If $I_p(\lambda)$ is the current density corresponding to wavelength λ, the photocurrent spectrum corresponding to a particular energy distribution can be obtained by multiplying the IPCE with the photon flux density of that distribution.

$$I_p(\lambda) = IPCE\ F(\lambda)d\lambda = IPCE\ P(\lambda)\ \lambda\left(\frac{e}{hc}\right) \tag{3.6.23}$$

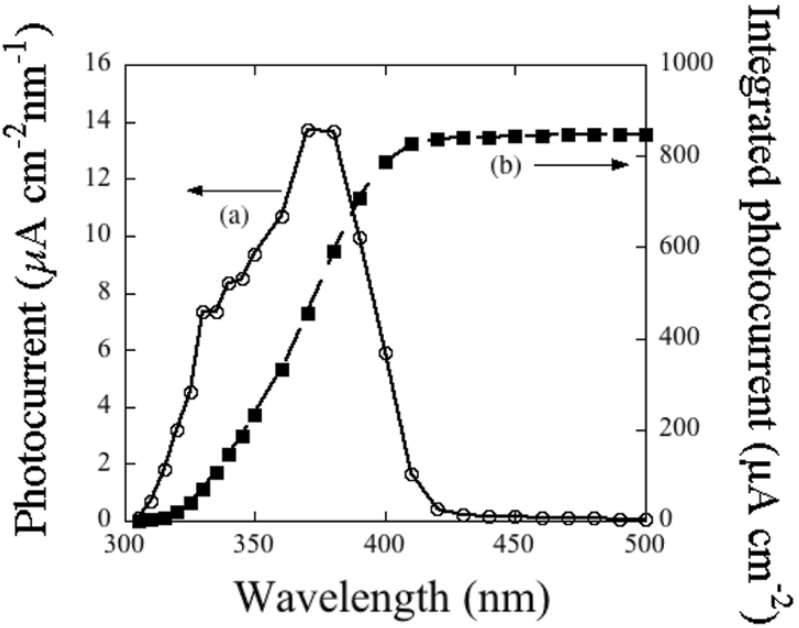

Fig. 3.25: (a) The solar photocurrent spectrum of a titania nanotube array obtained using data from **Fig. 3.19** and **Fig. 3.24**. **(b)** The total solar photocurrent obtained by integrated the photocurrent of **(a)**.

For example, the solar photocurrent spectrum of a titania nanotube array photoanode calculated using relation (3.6.23) is given in **Fig. 3.25**. The solar irradiance P (λ) for the calculation is taken from **Fig. 3.19**. The total photocurrent that can be obtained from this electrode when exposed to global sunlight is

$$I_p = \int_{\lambda_{\min}}^{\infty} I_p(\lambda)d\lambda \tag{3.6.24}$$

Curve **(b)** of **Fig. 3.25** is obtained by the integral of Curve **(a)**. As can be seen from Curve **(b)** of **Fig. 3.25**, I_p= 847 μA/cm^2. Outdoor measurements yielded values agreeing well with this calculated photocurrent value (State college, Pennsylvania; latitude 40.79°N, longitude 77.86°W, on April 3, 2007 at 3:00 PM, clear sky, incident irradiance 950 W/m^2).

Solar photoconversion efficiency can be calculated using relation (3.6.24) in (3.6.13).

$$\varepsilon_0 = \left(\frac{e}{hc}\right)\left(V_{rev}^0 - V_{bias}\right)\left(\frac{\int_{\lambda_{\min}}^{\infty} IPCE(\lambda)\,P(\lambda)\,\lambda\,d\lambda}{P_t}\right) \tag{3.6.25}$$

This modified form of relation (3.6.13) is the most acceptable relation for calculating the photoconversion efficiency [109,123,137]. With V_{bias}= 0.51 V, the solar photoconversion efficiency of titania nanotube (6 μm length) array photoelectrodes was calculated as 0.6 %.

Another parameter of interest, used mainly in photoelectrochemical solar cells is the absorbed photon to current conversion (APCE) efficiency. This is also called the internal quantum efficiency. APCE is defined as the number of electrons (or holes) collected per absorbed photon. It is calculated after considering the losses in the incident photons like reflection, scattering, absorption, etc. APCE and IPCE are related by [138]:

$$IPCE(\lambda) = LHE(\lambda)\,\phi_{inj}\,\eta \tag{3.6.26}$$

LHE is the light harvesting efficiency or absorptance, defined as LHE = 1-10^{-A} where A is the absorbance, ϕ_{inj} is the quantum yield of charge injection, and η is the efficiency of transporting injected electrons in to the external circuit. Equation (3.6.26) can be written as:

$$APCE = \frac{IPCE}{1-10^{-A}} \tag{3.6.27}$$

IPCE and APCE can have values close to 100%. As discussed before, the maximum attainable photoconversion efficiency in a single bandgap photoelectrolysis cell is 30.7%. Although stable, the photoconversion efficiencies of most oxide semiconductors are low (<2% except the case of 8.35% reported for carbon modified titania [121]) due to their large band gap.

References

1. Veziroğlu TN (2000) Quarter century of hydrogen movement. 25:1143–1150
2. Govindjee (Ed.)(1975) Bioenergetics of Photosynthesis. Academic Press, New York
3. Blankenship RE (2002) Molecular Mechanism of photosynthesis. Blackwell Science, Publishers, USA
4. Hall DO (1978) Solar energy conversion through biology—could it be a practical energy source? Fuel 57:322-333
5. Cuendet P, Grätzel M (1982) Artificial photosynthetic systems. Cellular and Molecular Life Sciences 38:223-228
6. Grätzel M (1982) Artificial photosysnthesis, energy-and light-driven electron transfer in organized molecular assemblies and colloidal semiconductors. Biochim Biophys Acta 683:221–244
7. Collings AF, Critchley C (Ed.) (2004) Artificial Photosynthesis-from basic biology to industrial application. Willey-VCH, Weinheim
8. Sun L, Hammarström, L, Akermark B, Styring S (2001) Towards artificial photosynthesis; ruthenium-manganese chemistry for energy production, Chem Soc Rev 30:36–39
9. Sun L, Akermark B, Hammarström, L, Styring S. (2003) Towards solar energy conversion into fuels; design and synthesis of ruthenium-manganese supramolecular complexes to mimic the function of photosystem II. In: utilization of Green house gases Liu CJ, Mallinson RG, Aresta M (Eds.) Amer Chem Soc Book Dept, Symposium Series No. 852, Washington USA, pp. 219–244
10. Lomoth R, Magnuson, A, Sjödin, Huang P, Styring S, Hammarström L (2006) Mimicking the electron donor side

of the photosystem II in artificial photosysnthesis. Photosysnthesis Res 87:25–40
11. Gerischer H (1979) Solar Photoelectrolysis with semiconductor electrodes. In: Solar energy conversion: Solid-state physics aspects, Seraphin BO (Ed). pp.115–172 Springer-Verlag New York
12. Vinodgopal K, Hotchandani S, Kamat PV (1993) Electrochemically assisted photocatalysis - TiO_2 particulate film electrodes for photocatalytic degradation of 4-chlorophenol. J Phys Chem 97:9040-9044
13. Hoffmann MR, Martin ST, Choi W, Bahneman DW (1995) Environmental applications of semiconductor photocatalysis. Chem Rev 95:69-96
14. Byrne JA, Eggins BR, Byers W, Brown NMD (1999) Photoelectrochemical cell for the combined photocatalytic oxidation of organic pollutants and the recovery of metals from waste waters. Appl Catal B: Environ 20:L85-89
15. Solarska R, Santato C, Jorand-Sartoretti C, M. Ulmann and J. Augustynski (2005) Photoelectrolytic oxidation of organic species at mesoporous tungsten trioxide film electrodes under visible light illumination. J Appl Electrochem 35:715–721
16. Quan X, Yang S, Ruan X, Zhao H (2005) Preparation of titania nanotube and their environmental applications as electrode. Envion Sci Technol 39:3770-3775
17. Nozik AJ (1980) Photoelectrochemical Cells. Phil Trans Royal Soc London Series 295:453-470
18. Heller A (1981) Conversion of sunlight into electric power and photoassisted electrolysis of water in photoelectron-chemical cells. Acc Chem Res 14:154-162
19. Memming R (1988) Photoelectrochemical solar energy conversion. Top Curr Chem 143:79-112
20. Nozik AJ, Memming R (1996) Physical Chemistry of semiconductor-liquid interface. J Phys Chem 100:13061–13078
21. Hill R, Archer MD (1990) Photoelectrochemical cells- a review of progress in the past 10 years. J Photo Chem Photo Biol A: Chem 51:45–54
22. Bolton JR (1996) Solar photoproduction of hydrogen: review. Sol Energy 57:37–50

23. Tryk, DA, Fujishima A, Honda K. Recent topics in photoelectrochemistry: achievement and future prospect (2000) Electrochim Acta 45:2363-2376
24. Bak T, Nowotny, J, Rekas M, Sorrell CC. (2002) Photoelectrochemical hydrogen generation from water using solar energy. Materials-related aspects. Int J Hydrogen Chem 991–1022
25. Aroutiounian VM, Arakelyan VM, Shahnazaryan GE (2005) Metal oxides photoelectrode for hydrogen generation using solar water radiation driven water splitting. Sol Energy 78:581–592
26. Fujishima A, Honda K (1972) Electrochemical photolysis of water at semiconductor electrode. Nature 238:37-38
27. Wrighton MS, Ellis AB, Wolczanski PT, Morse DL, Abrahamson HB, Ginley DS (1976) Strontium titanate photoelectrodes. Efficient photoassisted electrolysis of water at zero applied potential. J Am Chem Soc 98:2774–2779
28. Mavroides JG, Kafalas JA, Kolesar DF (1976) Photoelectrolysis of water in cells with $SrTiO_3$ anodes. Apl Phys Lett 28:241–243
29. Bicelli LP, Razzini G (1985) Photoelectrochemical performance of anodic n-TiO_2 films submitted to hydrogen reduction. Int J Hydrogen Energy 10:645–649
30. Jaramillo TF, Baeck SH, Shwarsctein AK, Choi KS, Stucky GD, McFarland EW (2005) Automatated electrochemical synthesis and photoelectrochemical characterization of $Zn_{1-x}Co_xO$ thin film for solar hydrogen production. J Comb Chem 7:264–271
31. Nozik AJ (1976) p-n photoelectrolysis cell. Appl Phys Lett 29:150–153
32. Ohashi K, McCann J, Bockris JOM (1977) Stable photoelectrochemical cell for splitting of water. Nature 266:610-611
33. Lee J, Fujishima A, Honda K, Kumashiro Y (1985) Photoelectrochemicl behaviour of p-type boron phosphide photoelectrode in acidic solution. Bull Chem Soc Jpn 58:2634-2637

34. Kainthala RC, Zelenay B, Bockris JOM (1987) Significant efficiency increase in self-driven photoelectrochemical cell for water photoelectrolysis. J Electrochem Soc 134:841–845
35. Nozik AJ (1977) Photochemical diodes. Appl Phys Lett 30:567–569
36. Nozik AJ (1975)Photoelectrolysis of water using semiconducting TiO_2 crystals. Nature 257:383–386
37. Mavroides JG, Tchernev DI, Kafalas JA, Kolesar DF (1975) Photoelectrolysis of water in cells with TiO_2 anodes. Mater Res Bull 10:1023–1030
38. Ohnishi T, Nakato Y, Tsubumura H (1975) Quantum yield of photolysis of water on titanium oxide. Ber Bunsenges Phys Chem 79:523–525
39. Kung HH, Jarrett HS, Sleight AW, Ferretti A (1977) Semiconducting oxide anodes in photoassisted electrolysis of water. J Appl Phys 48:2463–2469
40. Giordano N, Antonucci V, Cavallaro S, Lembo R, Bart JCJ (1982) Photoassisted decomposition of water over modified rutile electrodes. Int J Hydrogen Energy 7:867–872
41. Khan SUM, Al-shahry M, Ingler Jr. WB (2002) Efficient photochemical water splitting by a chemically modified n-TiO_2. Science 297:2243–2245
42. Fujishima A, Kohayakawa K, Honda K (1975). Hydrogen production under sunlight with an electrochemical photocell. J electrochem Soc 122:1487–1489
43. Akikusa J, Khan SUM (1997) Photo response and AC impedance characterization of n-TiO_2 during hydrogen and oxygen evolution in an electrochemical cell. Int J Hydrogen Energy 22:875–882
44. Bak T, Nowotny J, Rekas M, Sorrell CC (2002) Photoelectrochemical properties of TiO_2-Pt system in aqueous solutions. Int J Hydrogen Energy 27:19–26
45. Heller A and Vadimsky RG (1981) Efficient solar to chemical conversion: 12% efficient photoassisted electrolysis in the [p-type InP(Ru)/HCl-KCl/Pt(Rh)] cell. Phys Rev Lett 46:1153–1156

46. El Zayat MY, Saed MO, El Dessouki MS (1998) Photoelectrochemical properties of dye-sensitized Zr-doped $SrTiO_3$ electrodes. Int J Hydrogen Energy 23:259-266
47. Grätzel M (2001) The photoelectrochemical Cells. Nature 414:338-344
48. Carpetis C (1982) A study of water electrolysis with photovoltaic solar energy conversion. Int J Hydrogen Energy 7:287–310
49. Murphy OJ, Bockris JOM (1984) Photovoltaic electrolysis: Hydrogen and electricity from water and light. Int J Hydrogen Energy 9:557-561
50. Fischer M (1986) Review of hydrogen production with photovoltaic electrolysis system. Int J Hydrogen Energy 11:495–501
51. Siegel A, Schott T (1988) Optimization of photovoltaic hydrogen production. Int J Hydrogen Energy 13:659–675
52. Khaselev O, Turner JA (1998) A monolithic photovoltaic-photoelectrochemical device for hydrogen production via water splitting, Science 280:425–427
53. Rocheleau RE, Miller EL, Misra A (1998) High efficiency photoelectrochemical hydrogen production using multijunction amorphous photoelectrode. Energy & Fuels 12:3-10
54. Licht S, Ghosh S, Tributsch, H, Fiecher (2002) High efficiency solar energy water splitting to generate hydrogen fuel: probing RuS_2 enhancement of multiple band electrolysis. Sol Energy Mater Sol Cells 70:471-480
55. Harry LS, Wilson RH (1978) Semiconductor for photoelectrolysis Annu Rev Mat Sci 8:99-134
56. Bard AJ (1979) Photoelectrochemistry and heterogeneous photocatalysis at semiconductor. J Photochem 10:59-75
57. Wrighton MS (1979) Photoelectrochemical conversion of optical energy to electricity and fuels. Acc Chem Res 12:303-310
58. Nozik AJ (1978) Photoelectrochemistry: Applications to solar energy conversion. Annu Rev Phys Chem 29:189-122
59. Gerischer H (1981) The principles of photoelectrochemical energy conversion. In: Cardon F, Gomes WP, Dekeyser W

(Eds) Photovoltaic and photoelectrochemical solar energy conversion, Plenum, New York, pp. 199-245
60. Nozik AJ (1981) Photoelectrochemical devices for solar energy conversion. In: Cardon F, Gomes WP, Dekeyser W (Eds) Photovoltaic and photoelectrochemical solar energy conversion, Plenum, New York, pp. 263-312
61. Heller A (1984) Hydrogen-evolving solar cells. Science 233:1141-1148
62. Lewis NS (1990) Mechanistic studies of light-induced charge separation at semiconductor/ liquid interfaces. Acc Chem Res 23:176-183
63. Pleskov YV (1990) Solar energy conversion: a photoelectrochemical approach, Springer-Verlag, Berlin
64. Koval CA, Howard JN (1992) Electron transfer at semiconductor electrode-liquid electrolyte interfaces. Chem Rev 92:411-433
65. Memming R (1994) Photoinduced charge transfer processes at semiconductor electrodes and particles. Top Curr Chem 169:105-181
66. Sze SM (1981) Physics of semiconductor devices. John Wiley and Sons, New York
67. Neamen DA (2002) Semiconductor Physics and devices: basic principles 3rd Ed, Mc-Graw Hill professional, New York
68. Memming R (1983) Comprehensive treaties electrochemistry V. 7, Plenum press, New York
69. Gerischer H (1975) Electrochemical photo and solar cell principles and some experiments. J Electroanal Chem:Interfacial Electrochem 58:263-274
70. Gomer R, Tryson G (1977) An experimental determination of absolute half-cell emf's and single ion free energies of solvation. J Chem Phys 66:4413-4424
71. von Helmholtz HLF (1879) Studies of electric boundary layers Ann Phys Chem 7:337-382
72. Parsons R (1990) The electrical double layer: recent experimental and theoretical developments. Chem Rev 90:813-826

73. Bockris JOM, Khan SUM (1993) Surface Electrochemistry. A molecular level approach. Plenum Press, New York
74. Green M (1959) Electrochemistry of the semiconductor-electrolyte electrode. I The electrical double layer. J Chem Phys 31:200-203
75. Memming R (2002) Semiconductor electrochemistry. Wiley-VCH, Weinheim
76. Gerischer H (1970) Physical Chemistry: an advanced treatise. V.9A and V 4 Academic Press, New York
77. Gerischer H (1990) The impact of semiconductors on the concept of electrochemistry. Electrochim Acta 35:1677–1690
78. Memming R, Schwandt (1967) Potential and charge distribution at semiconductor electrolyte interface. Angew chem. Int Ed 6:851-861
79. Thapar R, Rajeshwar K (1983) Mott-Schottky analyses on n- and p-GaAs/room temperature chloroaluminate molten-salt interfaces. Electrochim Acta 28:195-198
80. Morrison SR (1980) Electrochemistry at semiconductor and oxidized metal electrodes. Plenum Press, New York
81. Bard AJ, Faulkner LR (1980) Electrochemical methods: Fundamental and applications, John Wiley and Sons, New York
82. Finklea HO (Ed.) (1988) Semiconductor electrodes; Studies in physical and theroretical chemistry. V. 55, Elsevier, NewYork
83. Chazalviel J (1988) Experimental techniques for the study of the semiconductor-electrolyte interface. Electrochim Acta 33:461-476
84. Chazalviel J (1990) Impedance studies at semiconductor electrodes: classical and more exotic techniques. Electrochim Acta 35:1545-1552
85. Marcus RA (1956) On the theory of oxidation reduction reaction involving electron transfer. J Chem Phys 24:966-978
86. Sutin N (1983) Theory of electron transfer reactions: Insights and hindsights. In: Prog Inorg Chem, Lippard SJ (Ed) 30:441-448, John Wiley & Sons, New York

87. Peter LM (1991) Dynamic aspects of semiconductor photoelectrochemistry. Chem Rev 90:753-769
88. Miller RDJ, Mclendon G, Nojik AJ, Schmickler W, Willing F (1995) Surface electron transfer Processes, VCH Publishers, New York
89. Lewis NS (1991) An analysis of charge transfer rate constant for semiconductor-liquid interfaces. Annu Rev Phys Chem 42:541
90. Lewis NS (1997) Progress in understanding electron transfer reaction at semiconductor/liquid interfaces. J Phys Chem B 102:4843-4855
91. Gerischer H (1991) Electron transfer kinetics of redox reactions at semiconductor/electrolyte contact: a new approach. J Phys Chem
92. Gao YQ, Gerogievskii Y, Marcus RA (2000) On the theory of electron transfer reactions at semiconductor/liquid interfaces. J Chem Phys 112:3358-3369
93. Smith BB, Nozik AJ (1996) Study of electron transfer at semiconductor-liquid interfaces addressing the full system electronic structure. Chem Phys 205:47-72
94. Smith BB, Halley JW, Nozik AJ (1996) On the Marcus model of electron transfer at immiscible liquid interface and its application to the semiconductor liquid interface. Chem Phys 205:245-267
95. Boroda YG, Voth GA (1996) A theory of adiabatic electron transfer processes across the semiconductor-electrolyte interface. J Chem Phys 106:6168-6183
96. Nishida M (1980) A Theoretical treatment of charge transfer via surface states at the semiconductor electrolyte interface. Analysis of water electrolysis process.
97. Tauc J (1970) Absorption edge and internal electric field in amorphous semiconductors. Mater Res Bull 5:721-729
98. Pankove JL (1971) Optical process of semiconductors. Prentice Hall, Englewood Cliffs, NJ, USA
99. Rajeshwar K (1993) Spectroscopy 8:16
100. Salvador P (2001) Semiconductor photoelectrochemistry: A kinetic and thermodynamic analysis in the light of

equilibrium and non-equilibrium models. J Phys Chem 105:6128–6141
101. Bird RE, Hulstrom RL, Lewis LJ (1983) Terrestrial solar spectral data sets. Solar energy 30:563-573
102. Bolton JR (1996) Solar photoproduction of hydrogen: A review. Solar Energy 57:37-50
103. Bolton JR, Strickler SJ, Connolly JS (1985) Limiting and realizable efficiencies of solar photolysis of water. Nature 316:495-500
104. Bolton JR (1978) Solar Fuels. Science 202:705-711
105. Archer MD, Bolton JR (1990) Requirements for ideal performance of photochemical and photovoltaic solar energy converters. J Phys Chem 94:8028-8036
106. Grimes DM; Grimes, CA (2006) A unique electromagnetic photon field using Feynman's electron characteristics and Maxwell's equations. J Computational and Theoretical Nanoscience 3:649-663
107. Shockley W, Queisser HJ (1961) Detailed balance limit of efficiency of p-n junction solar cells. J Appl Phys 32:510-519
108. Hanna MC, Nozik AJ (2006) Solar conversion efficiency of photovoltaic and photoelectrolysis cells with carrier multiplication absorbers. J Appl Phys 100: 074510 (8 pages)
109. Murphy AB, Barnes PRF, Randeniya LK, Plumb IC, Grey IE, Horne MD, Glasscock JA (2006) Efficiency of solar water splitting using semiconductor electrodes. Int J Hydrogen Energy 31:1999-2017
110. Gerischer H (1981) The principles of photoelectrochemical energy conversion. In: Cardon F, Gomes WP, Dekeyser W (Eds) Photovoltaic and photoelectrochemical solar energy conversion, Plenum, New York, pp. 199-245
111. Weber MF, Dignam MJ (1984) Efficiency of splitting water with semiconducting photoelectrodes. J Electrochem Soc 131:1258-1265
112. Heller A (1981) Conversion of sunlight into electrical power and photoassisted electrolysis of water in photoelectrochemical cells. Acc Chem Res 14:154-162

113. Fujishima A, Kohayakawa K, Honda K (1975) Hydrogen production under sunlight with an electrochemical photocell. J Electrochem Soc 122:1487-1489
114. Bard AJ, Faulkner LR (2001) Electrochemical methods: Fundamentals and applications. John Wiley & Sons, New Jersey
115. Parkinson B (1984) On the efficiency and stability of photoelectrochemical devices. Acc Chem Res 17:431-437
116. Ang PGP, Sammells AF (1984) Hydrogen evolution at p-InP photocathodes in alkaline electrolyte. J Electrochem Soc 131:1462-1464
117. Dohrmann JK, Schaaf NS (1992) Energy conversion by photoelectrolysis of water: determination of efficiency by in situ photocalorimetry. J Phys Chem 96:4558-4563
118. Heller A (1982) Electrochemical solar cells. Solar energy 29:153-162
119. Aharon-Shalom E, Heller A (1982) Efficient p-InP (Rh-H alloy) and p-InP (Re-H alloy) hydrogen evolving photocathodes. J Electrochem Soc 129:2865-2866
120. Heller A, Vadimsky RG (1981) Efficient solar to chemical conversion: 12% efficient photoassisted electrolysis in the [p-type InP(Ru)]/HCl-KCl/Pt(Rh) cell. Phys Rev Lett 46:1153-1156
121. Khan SUM, Al-shahry M, Ingler Jr. WB (2002) Efficient photochemical water splitting by a chemically modified n-TiO_2. Science 297:2243–2245
122. Lackner KS (2003) Comment on "Efficient photochemical water splitting by a chemically modified n-TiO_2" - (III). Science 301:1673c
123. Hagglund C, Gratzel M, Kasemo B (2003) Comment on "Efficient photochemical water splitting by a chemically modified n-TiO_2" - (II). Science 301:1673b
124. Fujishima A (2003) Comment on "Efficient photochemical water splitting by a chemically modified n-TiO_2" - (II). Science 301:1673a
125. Raja KS, Mahajan VK, Misra M (2006) Determination of photoconversion efficiency of nanotubular titanium oxide

photo-electrochemical cell for solar hydrogen generation. J Power Sources 159:1258-1265
126. Khan SUM, Akikusa J (1999) Photoelectrochemical splitting of water at nanocrystalline n-Fe_2O_3 thin-film electrodes. J Phys Chem B 103:7184-7189
127. Tomkiewicz M, Woodall JM (1977) Photoelectrolysis of water with semiconductor materials. J Electrochem Soc 124:1436-1440
128. Butler MA, Ginley DS (1980) Principles of photoelectrochemical, solar energy conversion. J Mater Sci 15:1-19
129. Nozik AJ (1975) Photoelectrolysis of water using semiconducting TiO_2 crystals. Nature 257:383-386
130. Wrighton MS, Ginley DS, Wolczanski PT, Ellis AB, Morse DL, Linz A (1975) Photoassisted electrolysis of water by irradiation of a titanium dioxide electrode. Proc Nat Acad Sci 72:1518-1522
131. Bockris JOM, Murphy OJ (1982-1983) The two efficiency expressions used in evaluating photo-assisted electrolysis. Appl Phys Commun 2:203-207.
132. Varghese, OK; Grimes, CA (2007) Appropriate Strategies For Determining The Photoconversion Efficiency Of Water Photoelectrolysis Cells: A Review With Examples Using Titania Nanotube Array Photoanodes. Solar Energy Materials and Solar Cells, in press.
133. Ghosh AK, Maruska HP (1977) Photoelectrolysis of water in sunlight with sensitized semiconductor electrodes. J Electrochem Soc 124:1516-1522
134. Bezman R, Fujishima A, Kohayakawa K, Honda K (1976) Hydrogen production under sunlight with an electro-chemical photocell. J Electrochem Soc 123:842-843
135. Kainthla RC, Zelenay B, Bockris JOM (1987) Significant efficiency increase in self-driven photoelectrochemical cell for water photoelectrolysis. J Electrochem Soc 134:841-845
136. Kay A, Cesar I, Gratzel M (2006) New Benchmark for water photooxidation by nanostructured α-Fe_2O_3 films. J Am Chem Soc 128:15714-15721

137. Bard AJ, Memming R, Miller B (1991) Terminology in semiconductor electrochemistry and photoelectrochemical energy conversion. Pure Appl Chem 63:569-596
138. Nazeeruddin MK, Kay A, Rodicio I, Humphry-Baker R, Muller E, Liska P, Vlachopoulos N, Gratzel M (1993) Conversion of light to electricity by cis-X_2Bis(2,2′-bipyridyl-4,4′-dicarboxylate)ruthenium(II) charge-transfer sensitizers (X=Cl^-, Br^-, I^-, CN^-, and SCN^-) on nanocrystalline TiO_2 electrodes. J Am Chem Soc 115:6382-6390